Earth and Space Science

RESEARCH ARTICLE
10.1029/2020EA001171

Geologic Map of the Niobe Planitia Region (I-2467), Venus

Iván López[1] **and Vicki L. Hansen**[2]

[1]Departamento de Biología y Geología, Física y Química Inorgánica, Universidad Rey Juan Carlos, Madrid, Spain,
[2]Department of Earth and Environmental Sciences, University of Minnesota-Duluth, Duluth, MN, USA

This article is a companion to Hansen and López (2020), https://doi.org/10.1029/2019EA001066.

Key Points:
- We present a geologic map of the Niobe Planitia region (0°N–57°N/60°E–180°E), representing about 13% of Venus' surface
- The map area displays an important imprint of the Artemis superstructure associated tectonic suites
- Different volcanic styles locally resurface the map area, where different basement materials record the history of an ancient era

Supporting Information:
- Plate S1

Correspondence to:
I. López,
ivan.lopez@urjc.es

Citation:
López, I., & Hansen, V. L. (2020). Geologic map of the Niobe Planitia region (I-2467), Venus. *Earth and Space Science*, *7*, e2020EA001171. https://doi.org/10.1029/2020EA001171

Received 12 MAR 2020
Accepted 16 JUN 2020
Accepted article online 16 JUL 2020

Abstract We present a 1:10M scale geologic map of the Niobe Planitia region of Venus (0°N–57°N/60°E–180°E). We herein refer to this area as the Niobe Map Area (NMA). Geologic mapping employed NASA Magellan synthetic aperture radar and altimetry data. The NMA geologic map and its companion Aphrodite Map Area (AMA) cover ~25% of Venus' surface, providing an important and unique perspective to study global and regional geologic processes. Both areas display a regional coherence of preserved geologic patterns that record three sequential geologic eras: the ancient era, the Artemis superstructure era, and the youngest fracture zone era. The NMA preserves a limited record of the fracture zone era, contrary to the AMA. However, the NMA hosts a diverse and rich assemblage of material and structures of the ancient era and structures that define the Artemis superstructure era. These two eras likely overlap in time and account for the formation of basement materials and lower plain units. Impact craters formed throughout the NMA recorded history. Approximately 40% of the impact craters show interior flood deposits, indicating that a significant number of NMA impact craters experienced notable geological events after impact crater formation. This and other geologic relations record a geohistory inconsistent with postulated global catastrophic resurfacing. Together, the NMA and the AMA record a rich geologic history of the surface of Venus that provide a framework to formulate new working hypotheses of Venus evolution and to plan future studies of the planet.

1. Introduction

NASA's Magellan mission collected near-global synthetic aperture radar (SAR) data of the surface of Venus between 1990 and 1994 and revolutionized the knowledge of our sister terrestrial planet. One of the main results of this first global reconnaissance of Venus is that our neighbor planet lacks a system of moving plates like the ones that operates here on Earth. However, an understanding of how Venus has evolved through time remains elusive. Paramount to unraveling the geodynamic evolution of a planet, Earth included, is to discover the structures, materials, and processes that have molded its surface, for which regional geologic mapping has proven to be a fundamental tool. Regional mapping provides a mean to document and synthesize our current knowledge of a region or planet and also serves as a tool to test working hypotheses, formulate questions, and devise new concepts to be studied in the future. A previous 1:10M global geologic map of Venus, including this study area, was carried out by Ivanov and Head (2011). The work presented here differentiates from this previous mapping in that the methodological approach followed here separates mapping of structures and units (e.g., Hansen, 2000; Hansen & López, 2018).

In this work we present a geologic map of the 1:10M Niobe Planitia Map Area (I-2467; 0°N–57°N/60°E–180°E). This map is part of a collaborative mapping project that includes the companion Aphrodite Map Area (AMA, I-2476), the object of a separate contribution (Hansen & López, 2020). Together, both maps cover >25% of Venus. The area includes different types of terrains, units, structures, and volcanic styles representative of the surface of Venus. The map scale is well-suited for the discovery of regional to global scale processes and to test current models of Venus geologic processes and evolution.

2. The Niobe Planitia Map Area (NMA)

The Niobe Planitia Region of Venus (I-2467) covers a surface of ~60,000,000 km^2 extending from lat 0°N to 57°N and from long 60° to 180°E (Figure 1). We refer to the map area as the Niobe map area, or NMA, herein. NMA takes its name from Niobe Planitia, a large volcanic lowland province that occupies the central map area.

10.1029/2020EA001171

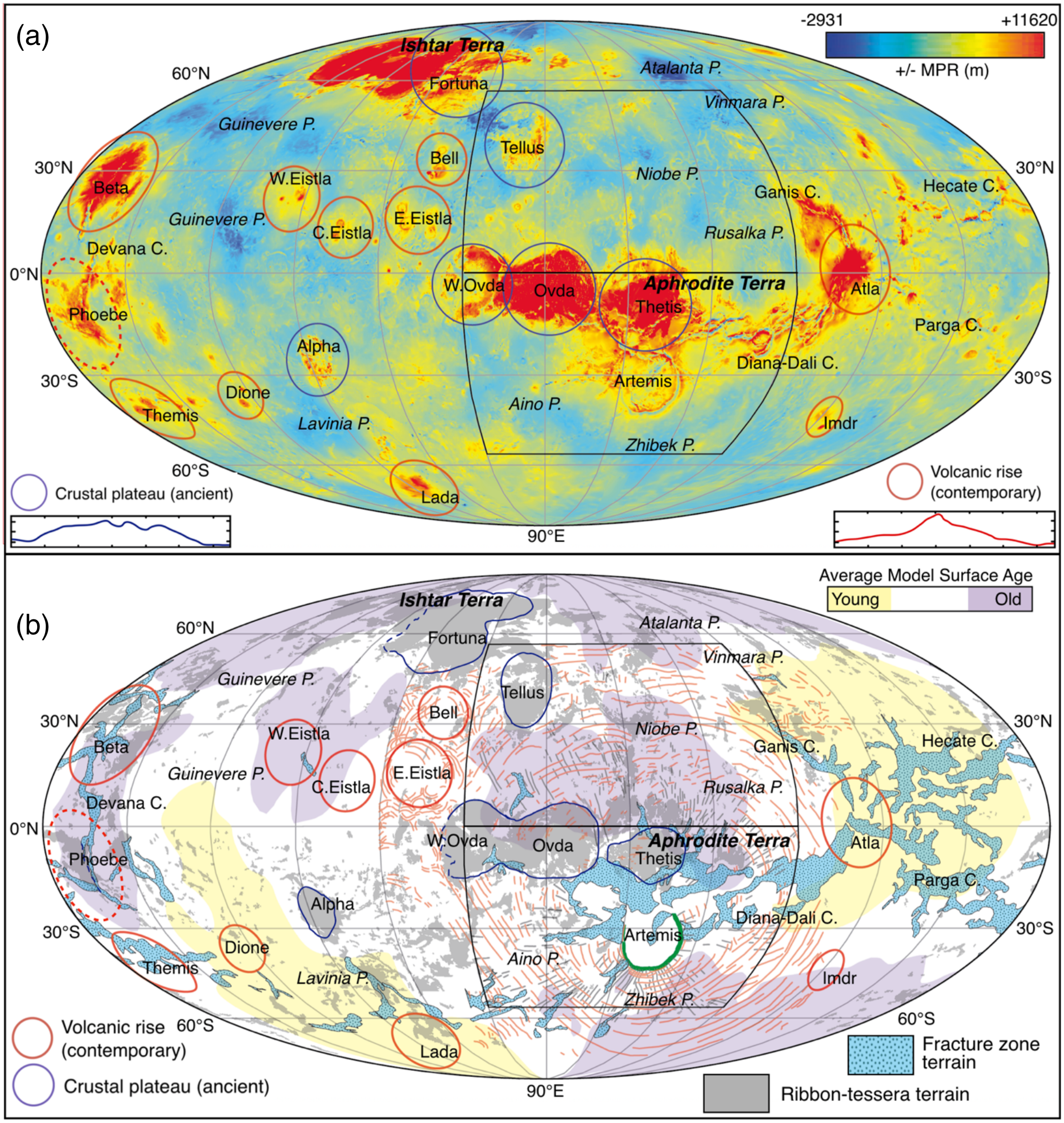

Figure 1. Mollweide projections of Venus; the NMA (north) and AMA (south) are shown as polygons. (a) Altimetry: highlands, red; mesolands, yellow; lowlands, blues; Ishtar Terra and Aphrodite Terra are composite highlands; highland features include crustal plateaus and volcanic rises, and hybrid Phoebe Regio. Planitiae are indicated by "P." and chasmata with "C." Topographic profiles (Ovda Regio, 90°E; Beta Regio 23.6°E), ~6 km vertical, 3,500 km horizontal. (b) Global distribution of average model surface age provinces (Hansen & Young, 2007; Phillips & Izenberg, 1995); fracture zone terrain ("rift" of Price & Suppe, 1995); ribbon-tessera terrain (Hansen & López, 2010); Artemis Chasma (green); trajectories of Artemis Chasma-radial fractures (gray lines) and wrinkle ridges (faded red lines), including Artemis Chasma-concentric wrinkle ridges and wrinkle ridges not concentric to Artemis (Hansen & Olive, 2010). Labels as in (a). Modified from Hansen (2018).

10.1029/2020EA001171

The NMA includes the northern part of western Aphrodite Terra, a topographically high region that extends ~10° (~1,000 km) on either side of the equator, including the crustal plateaus of western and central Ovda Regio and Thetis Regio, and several planitiae to the north. Tellus Regio, the third crustal plateau in the NMA, dominates the northwest NMA, defining the boundary between western planitiae. Elsewhere, ridge belts (also called deformation belts) and/or large tessera-terrain inliers, forming locally higher regions, define the boundaries between planitiae in northern, central, and eastern NMA.

Topographically the NMA ranges in altitude from over 5 km above mean planetary radius (MPR) in the equatorial highland regions to around 2.5 km below MPR in the lowlands of Leda and Atalanta Planitiae within northwestern and northeastern NMA, respectively. Llorona, Niobe, and Sologon Planitiae, located north of the equatorial crustal plateaus, may form the northern part of a broad Artemis-concentric topographic trough (Hansen & López, 2020). Akhtamar Planitia occupies southwestmost NMA, whereas Rusalka Planitia occupies the southeast corner. Northern NMA includes from east to west: Atalanta, Vellamo, Tilli-Hanum, Lowana, and Leda Planitiae.

Published 1:5 million-scale Venus geologic maps, so-called VMaps were used in the geologic mapping process (V23, I-3025 (Hansen, 2009); V24, I-3086 (Lang & Hansen, 2008); V25, I-2783 (Young & Hansen, 2003); V13, I-2870 (Ivanov & Head, 2005); V3, I-3018 (Ivanov & Head, 2008); V4, I-2792 (Ivanov & Head, 2004)). Other VMaps that spatially overlap with NMA were not published at the time that this geologic map went to review (e.g., V10, V11, V12, and V22). Other previous works on the study area were also considered for mapping and the discussion of the regional geology (e.g., Basilevsky & Head, 1996; Gilmore & Head, 2018; Herrick & MacGovern, 2000).

3. Data and Methods

3.1. Image Data

Data for this study were provided by the U.S. Geological Survey (USGS) Astrogeology Team in the projection parameters (Mercator projection) for the Niobe Planitia Region (I-2467). The data are available online from the USGS Map-a-planet website (https://astrocloud.wr.usgs.gov/).

Cycle 1 (east-directed illumination or left-looking) SAR images cover essentially the entire I-2467 map area, with local data gaps, particularly within central NMA. Cycle 2 (west-directed illumination or right-looking) SAR data cover western NMA (60°E–120°E); cycle 3 left-look stereo SAR data are scarce and banded (Ford et al., 1993). Digital Compressed Once Mosaicked Image Data Records (C1-MIDR; 225 m/pixel) SAR data from the regional database and map base and digital full-resolution radar map (FMAP; 75–125 m/pixel) data set were used in constructing the geologic map.

We also employed other ancillary non-SAR Magellan data available through the USGS Map-A-Planet website. The data sets include (a) Topography (Global Topographic Data Record 3; GTDR 3); (b) Slope data (Global Slope Data Record; GSDR); (c) Reflectivity (Global Reflectivity Data Record; GRDR); and (d) Emissivity (Global Emissivity Data Record; GEDR).

GTDR data have an effective horizontal resolution of 10 km and were combined with SAR images to produce synthetic stereo anaglyphs (Kirk et al., 1992) using NIH-Image macros developed by D. A. Young. Synthetic stereo images played a critical role in elucidating the relations between geology and topography and, in particular, the interaction of flows, primary and secondary structures, and topography.

3.2. Image Interpretation and Geologic Mapping

The interpretation of features in SAR images is key to developing a NMA geologic history. Ford et al. (1993) explored the subject of SAR image interpretation in depth. The methodology for defining geologic units and structural fabrics builds on standard geologic analysis detailed by Wilhelms (1990) and Tanaka et al. (1993) and employs cautions of Hansen (2000), Zimbelman (2001), Skinner and Tanaka (2003), and McGill and Campbell (2004). Map units represent material emplaced within an increment of geologic history to which standard stratigraphic methods have some limited application. Other units may be composite, in that the units might not be stratigraphically coherent over the entire represented area and (or) the material may have been emplaced over an extended period of time, particularly in relation to other units and (or) formation of secondary structures. In such cases the map units are descriptive units rather than temporal units. Attempts were made to clearly separate secondary structures from material units; location, orientation, and relative density of primary and secondary structures are shown independent of material units. Evidence for reactivation of secondary structures is common across the map area, which further complicates the process of unraveling both temporal constraints and geologic history. In addition, in many cases the designation of a material unit does not carry an implication of concurrent or synchronous emplacement (e.g., Hansen, 2000). Indeed, absolute time is essentially impossible to constrain with regard to Venus geology at the time of this study.

Criteria for distinguishing discrete geologic units in the map area include (but are not limited to) (1) the presence of sharp, continuous contacts; (2) truncation of, or interaction with, underlying secondary structures and topography; and (3) primary structures, for example, flow channels or edifice topography, that allow a reasonable geologic interpretation and which may also provide clues to three-dimensional geometry. Some mapped units do not fit these constraints, which limits their use in constructing stratigraphic interpretations. Composite units, in particular, do not provide reasonable temporal constraints, even of a relative nature. Composite character of the units is noted in the description of map units.

Estimating absolute geologic age is not currently possible for the surface of Venus. Unlike surface crater statistics for planetary bodies that have old surfaces and high crater densities, such as the Moon and Mars, Venus impact crater statistics cannot place constraints on the age of surface units that cover the small areas visible in the map area given the low density of craters and lack of small craters (Campbell, 1999; Hauck et al., 1998; McKinnon et al., 1997). Relative age constraints may be established only where units are in mutual contact and (or) interact with the same suite of secondary structures. Such relative temporal constraints are only locally applicable and cannot be extended across the map area with confidence nor are they valid for composite (time-transgressive) geologic units.

Geologic maps at all scales should provide the basis for interpreting geologic histories, which in turn provide critical relations for understanding the range of processes that contributed to the evolution of planets. Construction of a geologic map is a critical first step in unraveling geologic history. Geologic maps are interpretive products used in turn for further interpretation of geological processes (Butler & Bell, 1988; Maltman, 1990). Therefore, mapping must be conducted in a fashion that ensures that any operative process can be discovered—that is, the mapping method must not predetermine the resulting geologic map (Hansen, 2000). It is imperative, for example, that secondary structures (strain) be distinguished from geologic units because materials and structures record different "time slices" in the evolution of Venus' surface, and each reflect different aspects of the operative processes which formed overall geology (Easton et al., 2005, 2016; Hansen, 2000; Wilhelms, 1972, 1990). In the construction of this map we attempt to adhere to historical and contemporary terrestrial mapping methods, with particular attention to complementary criteria, format, and cautions outlined for Venus (e.g., Butler & Bell, 1988; Compton, 1985; Gilbert, 1886; Grindrod & Guest, 2006; Hansen, 2000; Hansen & López, 2018; Maltman, 1990; McGill & Campbell, 2004; Skinner & Tanaka, 2003; Tanaka et al., 1993, 2010; Wilhelms, 1972, 1990; Zimbelman, 2001).

In this contribution we identify and map (a) geomorphic features and named features within the map area; (b) primary and secondary structures, most commonly lineaments formed during unit emplacement, or after unit emplacement, respectively; (c) material units; (d) non-material units such as ribbon-tessera terrain or shield terrain (e.g., lithodemic units; Easton et al., 2005, 2016); and (e) shock features or thin deposits that overlay material units or terrains (e.g., impact crater haloes and mantling material), shown as transparent stippled areas.

4. The NMA Geologic Map

This section describes the NMA geologic map (Plate 1; see also Supporting Information Plate S1). The NMA is composed of an assemblage of materials and structures that together record a spatially and temporally varied geohistory: (a) local basal terrains (crustal plateaus, lowland tessera inliers, and other local basal units); (b) a suite of geological elements—tectonic and magmatic—associated with the formation of the Artemis superstructure (Hansen & Olive, 2010); (c) regionally extensive suites of tectonic structures exposed across the lowlands and local tectonic suites associated with individual tectonomagmatic features; (d) volcanic

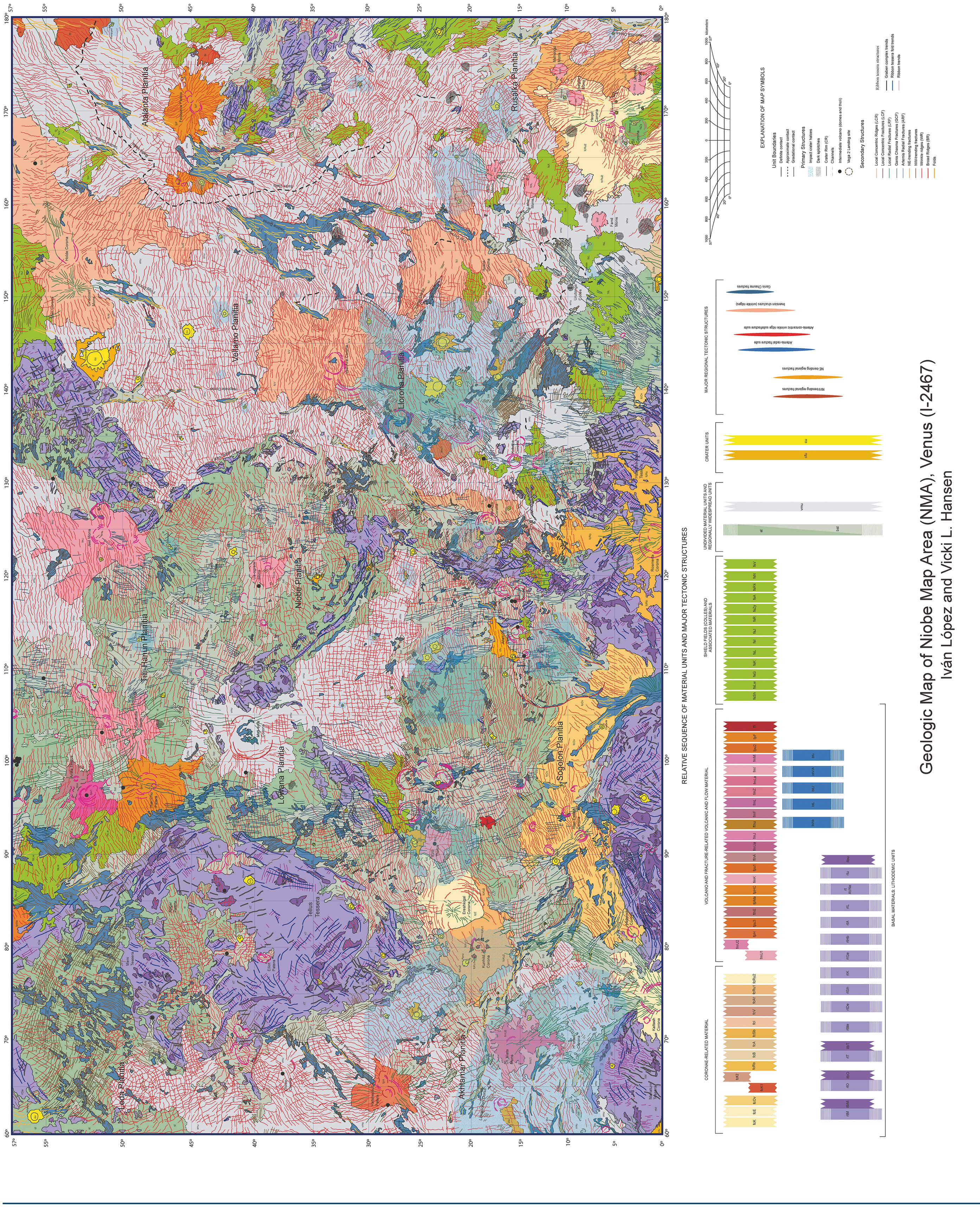

Plate 1. Geologic Map of the Niobe Planitia Region (I-2467), Venus. See also Supporting Information Plate S1.

DESCRIPTION OF MAP UNITS

Unit label	Unit name	Unit definition	Interpretation	Correlative units or notes
		CRATER MATERIAL		
cfu	**crater associated flow material, undivided**	Moderately high backscatter; digitate flow fronts.	Impact melt or fluidized ejecta created by meteorite impact associated with the formation of individual impact craters.	This unit is descriptive with no implications for temporal equivalence across the map area.
cu	**Crater material, undivided**	High backscatter material surrounding a central depression, rim materials, and floor materials of radar-bright and radar-dark varieties; exterior deposits typically lobate, with patchy radar image texture and bright streaks radial to the central cavity.	Deposits and structures created by meteorite impact, including impact melt, fluidized ejecta, or subsurface magma. Crater formed by impact onto the surface. Hummocky texture of near-rim material reflects distribution of continuous ejecta. Radar bright floors may be fractured impact melt, while radar-dark floors may reflect post-emplacement volcanic flooding or smooth impact melt.	This unit is descriptive with no implications for temporal equivalence across the map area.
		VOLCANO-RELATED UNITS		
fpMa	**Malintzin Patera flow material**	Medium- to high-radar-backscatter materials in the vicinity of Malintzin Patera.	Volcanic flows associated with Malintzin Patera.	Deformed by ACWR.
fthA	**Amra Tholus flow material**	Medium- to high-radar-backscatter materials associated with Amra Tholus; overlapping packages of lobate morphology and variable backscatter; several regions of high backscatter occur around the edifice.	Volcanic flows associated with Amra Tholus. High-back scatter packages represent high viscosity flows (i.e. festoon flows).	Locally cut by concentric fractures associated with Amra Tholus; Deformed by ACWR.
fthE	**Ezili Tholus flow material**	Medium- to high-radar-backscatter materials associated with Ezili Tholus; multiple overlapping packages radial to the central edifice; distal packages marked by high backscatter; numerous small shields distributed around the volcano; hummocky terrain locally around edifice. Medium backscatter material with highly digitate margins.	Volcanic materials associated with Ezili Tholus and nearby small shields; hummocky terrain represents collapse deposits.	Deformed by ACWR; some N-trending wrinkle ridges interpreted as ARF inversion structures (DeShon et al., 2000).
fpHC	**Hiei Chu Patera flow material**	Medium- to high-radar-backscatter materials associated with Hiei Chu Patera; multiple overlapping packages radial to volcanic center; numerous small shields around volcano.	Volcanic materials associated with Hiei Chu Patera and nearby small shields.	Deformed by local radial and concentric fractures and wrinkle ridges.
fmK	**Flow materials around Kurukulla Mons**	Mottled, medium- to high-radar-backscatter materials associated with Kurukulla Mons and other nearby unnamed volcanic centers; local high-backscatter lobate flows and steep-sided domes; numerous small shields around the edifice.	Volcanic materials associated with Kurukulla Mons, other intermediate volcanic centers, and small shields.	Deformed by local radial and concentric fractures and ACWR. Some wrinkle ridges interpreted as ARF inversion structures (DeShon et al., 2000).
fmJ	**Jael Mons flow material**	Medium- to high-radar-backscatter volcanic materials associated with Jael Mons and other nearby unnamed volcanic centers; multiple overlapping flows radial to the volcanic center; numerous small shields distributed around the edifice.	Volcanic materials principally associated with Jael Mons, other intermediate volcanic centers, and nearby small shields.	Deformed by local concentric fractures, regional fractures and ACWR.
fpF	**Fedosova Patera flow material**	High-radar-backscatter materials associated with Fedosova Patera; lobate flows radial to the volcanic center.	Volcanic materials associated with Fedosova Patera.	Deformed by wrinkle ridges with different trends, those radial to the volcanic center could represent inversion structures (DeShon et al., 2000)
fpH	**Hatshepsut Patera flow material**	Medium- to high-radar- backscatter volcanic materials associated with Hatshepsut Patera; multiple overlapping lobate flows of variable backscatter; numerous small shields distributed around the volcano.	Volcanic materials associated with Hatshepsut Patera.	
fmM	**Muhongo Mons flow material**	Mottled, medium-radar-backscatter material associated with Muhongo Mons; numerous individual flow units radiating from summit of mons and discrete shield patches.	Volcanic flows associated with Muhongo Mons and nearby small shields.	Deformed by NNW-trending wrinkle ridges.
fmI	**Iseghey Mons flow material**	Mottled, medium-radar-backscatter material associated with Iseghey Mons; numerous individual flow units radiating from summit of mons.	Volcanic flows associated with Iseghey Mons.	Deformed by N-trending wrinkle ridges.
fmLa	**Lamatsu Mons flow material**	Mottled, medium-radar-backscatter material associated with Lamashtu Mons; individual flow units radiating from the volcanic center.	Volcanic flows associated with Lamashtu Mons.	Deformed by NNW-trending wrinkle ridges.
fmF	**Fand Mons flow material**	Mottled, medium-radar-backscatter material associated with Fand Mons; numerous individual flows radiating from the volcanic center.	Volcanic flows associated with Fand Mons.	Deformed by local NE-trending regional fractures and NW-trending wrinkle ridges.
fmL	**Lahar Mons flow material**	Mottled, medium-radar-backscatter material associated with Lahar Mons; numerous individual flow units radiating from the volcanic center.	Volcanic flows associated with Lahar Mons.	Deformed by ACWR.
fmZ	**Zaltu Mons flow material**	Mottled, medium-radar-backscatter material associated with Zaltu Mons; numerous individual flow units radiating from the volcanic center.	Volcanic flows associated with Zaltu Mons.	Deformed by local radial fractures and ACWR.
fmU1	**Uti Hiata Mons flow material 1**	Mottled, low- to high-radar-backscatter materials associated with Uti Hiata Mons and other volcanic edifices; multiple overlapping lobate flows around Uti Hiata and flow materials from unnamed tholus to the south; numerous small shields and pits distributed around the volcano.	Proximal volcanic flows associated with Uti Hiata Mons and volcanic flows associated with nearby volcanic edifices.	Deformed by NE-trending wrinkle ridges (possible ACWR).Original characteristics are difficult to determine due to the presence of a crater halo.
fmU2	**Uti Hiata Mons flow material 2**	Mottled, low- to high-radar-backscatter materials associated with Uti Hiata Mons and other volcanic edifices; multiple overlapping lobate flows around Uti Hiata and flow materials from unnamed tholus to the south; numerous small shields and pits distributed around the volcano.	Proximal volcanic flows associated with Uti Hiata Mons and volcanic flows associated with nearby volcanic edifices.	Deformed by local radial and concentric fractures; locally bury ACWR.
fmUa	**Ua-ogrere Mons flow material**	Mottled, medium- to high-radar-backscatter materials associated with Ua-ogrere Mons and adjacent volcanic edifices; domes, numerous shields and pits distributed in and around volcanic structure.	Volcanic flows associated with Ua-ogrere Mons and its associated volcanic edifices.	Deformed by local concentric fractures; deformed by NE-trending regional fractures, ARF suite and ACWR.
fpu1	**unnamed patera 1 flow material**	Mottled, medium-radar-backscatter materials associated with unnamed patera located at 52°N/96°E; domes, numerous shields and pits distributed in and around volcanic structure.	Volcanic flows associated with the unnamed patera located at 52°N/96°E and its associated volcanic edifices.	Deformed by local concentric fractures associated with the patera; deformed by ACWR.
fpu2	**unnamed patera 2 flow material**	Mottled, medium-radar-backscatter materials associated with overlapping unnamed paterae located at 46°N/162°E.	Volcanic flows associated with the unnamed paterae located at 46°N/162°E.	Deformed by local concentric fractures associated with the patera; deformed by ACWR.
fpu3	**unnamed patera 3 flow material**	Mottled, medium- to high-radar-backscatter materials associated with unnamed patera located at 18.5°N/94°E.	Volcanic flows associated with the unnamed patera located at 18.5°N/94°E.	Deformed by local concentric fractures associated with the patera; deformed by ARF and ACWR.
fth1	**unnamed tholi 1 flow material**	Mottled, medium-radar-backscatter materials associated with unnamed tholi located at 23°N/134°E.	Volcanic flows associated with the unnamed tholi located at 23°N/134°E.	Deformed by local concentric fractures associated; deformed by ACWR.
ffr	**fracture-fed flow material**	Mottled, medium- to high-radar-backscatter materials associated with fractures in Atalanta Planitia.	Volcanic flows associated with fractures.	Deformed by NE-trending wrinkle ridges and folds.
		SHIELD FIELDS (COLLES) AND RELATED UNITS		
fsZy	**Zaryanitsa Dorsa shield field and associated flow materials**	Low-radar-backscatter materials formed by clusters of individual ~30-kilometer-diameter edifices and associated flows. Gradational contacts with surrounding units due to the point-source nature of shield volcanism.	Late stage local shield-sourced volcanism associated with corona evolution.	Deformed by local corona-related radial fractures and wrinkle ridges of variable trend.
fsR	**Ran Colles shield field and associated flow materials**	Low-radar-backscatter materials formed by clusters of individual ~30-kilometer-diameter edifices and associated flows. Gradational contacts with surrounding units due to the point-source nature of shield volcanism.	Local volcanic shield clusters and associated materials.	Deformed by NE-trending regional fractures and N-trending wrinkle ridges.
fsA	**Asherat Colles shield field and associated flow materials**	Mottled low- to medium-radar-backscatter materials formed by clusters of individual ~30-kilometer-diameter edifices and associated flows. Gradational contacts with surrounding units due to the point-source nature of shield volcanism.	Local volcanic shield clusters and associated materials.	Deformed by ACWR; some NNE-trending wrinkle ridges interpreted as ARF inversion structures (DeShon et al., 2000).
fsL	**Llorona Planitia shield field and associated flow materials**	Mottled low- to medium-radar-backscatter materials formed by clusters of individual ~30-kilometer-diameter edifices and associated flows. Gradational contacts with surrounding units due to the point-source nature of shield volcanism.	Local volcanic shield clusters and associated materials.	Some outcrops are cut by ARF, and others bury ARF (and are locally reactivated as inversion structures)
fsRk	**Rusalka Planitia shield field and associated flow materials**	Medium-radar-backscatter materials formed by clusters of individual ~30-kilometer-diameter edifices and flows surrounding Romanskaya crater. Gradational contacts with surrounding units due to the point-source nature of shield volcanism.	Local volcanic shield clusters and associated materials.	Deformed by NNW-trending wrinkle ridges and cut by NE-trending scarps of the west termination of Ganis Chasma.
fsI	**Ituana Corona shield field and associated flow materials**	Low-radar-backscatter materials formed by clusters of individual ~30-kilometer-diameter edifices and associated flows. Gradational contacts with surrounding units due to the point-source nature of shield volcanism.	Local volcanic shield clusters associated with Ituana Corona.	
fsJ	**Jurate Colles shield field and associated flow materials**	Medium-radar-backscatter materials formed by clusters of individual ~30-kilometer-diameter edifices and associated flows. Gradational contacts with surrounding units due to the point-source nature of shield volcanism.	Local volcanic shield clusters and associated materials.	Locally deformed by regional wrinkle ridges of variable trend. Shield clusters present a time-transgressive relation with wrinkle ridges and postdate the fractures.
fsV	**Vedma Dorsa shield field and associated flow materials**	Medium-radar-backscatter materials formed by clusters of individual ~30-kilometer-diameter edifices and associated flows. Gradational contacts with surrounding units due to the point-source nature of shield volcanism.	Local volcanic shield clusters and associated materials.	Locally deformed by regional wrinkle ridges of variable trend and NE-trending folds. Shield clusters present a time-transgressive relation with wrinkle ridges.
fsN	**Shield field and associated flow materials near Nemesis Tesserae**	Mottled medium-radar-backscatter materials formed by clusters of individual ~30-kilometer-diameter edifices and associated flows. Intermediate domes locally. Gradational contacts with surrounding units due to the point-source nature of shield volcanism.	Local volcanic shield clusters and associated materials.	Deformed by local concentric topographic rims/folds and regional wrinkle ridges of variable trend.
fsK	**Shield field and associated flow materials around Kubebe Corona**	Mottled medium-radar-backscatter materials formed by clusters of individual ~30-kilometer-diameter edifices and associated flows. Intermediate domes locally. Gradational contacts with surrounding units due to the point-source nature of shield volcanism.	Local volcanic shield clusters and associated materials.	Deformed by ARF, and ACWR. Deformation and shield emplacement is contemporaneous. Possible reactivation of older NW-trending regional fractures.
fsG	**Shield field and associated flow materials near Gegute Tessera**	Medium-radar-backscatter materials formed by clusters of individual ~30-kilometer-diameter edifices and associated flows; reticulate texture locally. Gradational contacts with surrounding units due to the point-source nature of shield volcanism.	Local volcanic shield clusters and associated materials.	Deformed by NE-trending regional fractures, ARF and ACWR. Shields postdate NE-trending fractures and are emplaced contemporaneously to N-trending fractures. Shields locally postdate the annulus of coronae (e.g. Allatu Corona).
fsSh	**Shield field and associated flow materials around Shimti Tessera**	Medium-radar-backscatter materials formed by clusters of individual ~30-kilometer-diameter edifices and associated flows. Gradational contacts with surrounding units due to the point-source nature of shield volcanism.	Local volcanic shield clusters and associated materials.	Deformed by ACWR and N-trending wrinkle ridges that are interpreted as inversion structures (e.g. DeShon and others, 2000).
fsLw	**Lowana Planitia shield field and associated flow materials**	Moderately High- to moderately low-radar-backscatter materials; densely populated by shield-type edifices, displays some digitate flow fronts and structural facies margins in distal regions.	Local volcanic shield clusters and associated materials.	Deformed by NE-trending regional fractures and ACWR. Locally some NE-trending wrinkle ridges are continuous with NE-trending regional fractures and interpreted as inversion structures (e.g. DeShon and others, 2000).
		CORONA-RELATED MATERIAL		
fcA	**Abundia/Nintu corona flow materials**	High- to low-radar-backscatter materials associated with Abundia and Nintu coronae; radar character difficult to define due to the presence of halo crater material; numerous small shields locally; local reticulate texture.	Volcanic materials related to corona- and volcano-associated volcanism.	Deformed by fractures concentric to coronae and ACWR.
fcAt	**Atalanta Planitia corona flow materials**	Medium- to high-radar-backscatter materials associated with Holde and Mari coronae and Cinacoatl Mons; composite unit of multiple overlapping flows where individual materials from the different volcano-tectonic features cannot be differentiated; numerous small shields locally.	Volcanic materials related to Abundia and Nintu coronae formation.	Deformed by fractures radial to Cinacoatl Mons and fractures concentric to Holde Corona. Deformed by ACWR suite and NNW-trending wrinkle ridges interpreted as ARF inversion structures (i.e. DeShon and others, 2000).
fcB	**Blai Corona flow materials**	Medium-radar-backscatter flows associated with Blai Corona; smooth to local lobate primary flow structures preserved; lies distal to Blai Corona in V–24 (Lang and Hansen, 2010).	Volcanic materials related to Blai Corona formation.	Deformed by local radial fractures. Correlative with unit fBa in Aphrodite map (Hansen and López, 2020).
fcE	**Ereshkigal Corona flow materials**	Medium- to high-radar-backscatter materials associated with Ereshkigal Corona; multiple overlapping lobate flows radial to the center of Ereshkigal Corona; numerous small shields and pits locally.	Volcanic materials related to Ereshkigal Corona formation.	Deformed by local radial fractures and concentric ridges, ACWR and NNW-trending wrinkle ridges interpreted as ARF inversion structures (i.e. DeShon and others, 2000).
fcI	**Ituana Corona flow materials**	Medium- to high-radar-backscatter lobate flow units from Ituana Corona in V–25 (Young and Hansen, 2003); kilometer-scale reticulate ridge patterns locally; includes Tie Fluctus and Praurime Fluctus and volcanic channels (e.g. Martuv Vallis).	Volcanic materials related to Ituana Corona formation.	Deformed by ridges concentric to the corona, ACWR, and NNW-trending wrinkle ridges interpreted as ARF inversion structures (i.e. DeShon and others, 2000).
fcK	**Kaltash Corona flow materials**	Smooth, medium-radar-backscatter materials associated with Kaltash Corona.	Volcanic materials related to Kaltash Corona formation.	Locally cut by fractures radial and concentric fractures to Kaltash Corona and other volcanic structures. Correlative with unit fKa in Aphrodite map (Hansen and López, 2020).

Unit label	Unit name	Unit definition	Interpretation	Correlative units or notes
fcK1	**Kunhild Corona flow materials 1**	Medium- to high-radar-backscatter materials associated with the early stages of Kunhild Corona formation located in the central part of the volcano-tectonic feature; local pits and caldera structures.	Early volcanic materials related to Kunhild Corona formation.	Deformed by the local radial fractures formed in the initial stages of the corona.
fcK2	**Kunhild Corona flow materials 2**	Medium- to high-radar-backscatter materials associated with Kunhild Corona; multiple overlapping lobate flows radial to the center of Kunhild Corona; locally flows emerged from fractures radial to the center of the corona; numerous small shields and pits locally.	Volcanic materials related to Kunhild Corona formation.	Deformed by local radial fractures and local concentric fractures and ridges. Distal flows deformed by ACWR.
fcOv	**Ovda Regio corona flow material, undivided**	Smooth, high- to low-radar-backscatter materials from different volcanotectonic structures (e.g. Habonde Corona, Atse Estsan Corona, Hansen, 2009); multiple pits and other primary structures indicative of subsurface lava flow.	Materials associated with the regional fracture zone/corona-chasmata system that cuts the Niobe and Aphrodite map area from east to west.	Deformed by local corona-related concentric fractures, NE-trending lineaments (fractures and pit chains) associated with the regional fracture zone/corona-chasmata, ARF and wrinkle ridges of variable trend.
fcR	**Rosmerta Corona flow material.**	Mottle to homogeneous, medium- to moderately low-radar-backscatter materials (Lang and Hansen, 2010); multiple pits and other primary structures indicative of subsurface lava flow.	Volcanic materials related to Rosmerta Corona formation.	Deformed by local radial and concentric corona-related fractures and by ACWR suite in distal flows. Correlative with unit fR in Aphrodite map (Hansen and López, 2020).
fcS	**Seia Corona flow material.**	Mottled to homogeneous, low-radar-backscatter materials from Seia Corona in V–37 (Hansen and DeShon, 2002).	Volcanic materials related to Seia Corona formation.	Deformed by fractures concentric to corona, ARF and ACWR. Correlative with unit fSa in Aphrodite Map area (Hansen and López, 2020).
fcV	**Ved-Ava Corona flow material.**	Medium- to high-radar-backscatter materials associated with Ved-Ava Corona; numerous small shields locally.	Volcanic materials related to Ved-Ava Corona formation.	Deformed by fractures concentric to the corona. Deformed by ACWR suite and NNW-trending wrinkle ridges interpreted as ARF inversion structures (i.e. DeShon and others, 2000).
fcRu1	**Rusalka Planitia corona flow materials 1**	Medium-radar-backscatter materials, topographically smooth volcanic material (Young and Hansen, 2003).	Volcanic materials related to corona-associated volcanism within Rusalka Planitia.	Deformed by NNW-trending wrinkle ridges. Truncates Baltis Vallis; locally blends into unit vmu (volcanic materials, undivided).
fcRu2	**Rusalka Planitia corona flow materials 2**	High-radar-backscatter materials associated with Eigin Corona, Hannahannas Corona, Heqet Corona and Saureu Corona in V–25 and V–37 (Hansen and DeShon, 2002; Young and Hansen, 2003); composite unit of multiple overlapping flows; materials from different volcano-tectonic features can not be differentiated; local kilometer-scale reticulate ridge patterns; includes Argimpasa Fluctus and volcanic channels.	Volcanic materials related to corona-associated volcanism within Rusalka Planitia.	Deformed by local concentric and radial corona-related fractures and wrinkle ridges and folds of variable trend. Correlative with unit fE in Aphrodite map (Hansen and López, in review).
fcSb	**Seia Corona flow materials b**	Moderately low to moderately high backscatter, digitate and lobate flow margins; sourced from fractures associated with Seia Corona.	Volcanic materials related to Seia Corona formation.	Correlative with unit fSb in Aphrodite map (Hansen and López, 2020).
		UNDIVIDED FLOW MATERIAL		
vmu	**volcanic material, undivided**	Undivided, low to moderate-radar-backscatter materials that can not be differentiated; discontinuous radar-boundaries; locally pock-marked by small shield edifices (typically less than 5 km in diameter); local pit chains and magmatic troughs.	Composite of individual local to regional volcano-magmatic events.	Deformed by different local and regional suites of fractures and wrinkle ridges.
		BASAL AND SHIELD MATERIAL AND/OR TERRAINS		
bst	**basal-shield transitional terrain, undivided**	Medium- to low-radar-backscatter material of heterogeneous texture, variably mottled to lineated region, characterized by both numerous shields (generally less than 5 km diameter) and other larger volcanic features (e.g. paterae, mons, tholus and small coronae). Contacts with unit st are locally interdigitate and difficult to determine due to the point-sourced nature of both units.	Regions of variably, generally shallow cover of pre-existing basal terrain deformed by extensional lineament suites; spotty, inconsistent cover consists of a thin discontinuous patchwork layer of shields (e.g., 'shield paint' of Hansen, 2005); these shield cover materials are in turn variably deformed by wrinkle ridges that form part of a regional suite concentric to Artemis (Hansen and Olive, 2010). This unit is transitional between the basal terrain and shield terrain; as its name implies, and it commonly lies adjacent to either or both of these units.	Deformed by suites of variably preserved/developed lineament trends and by regional wrinkle ridges.There is no implication of temporal correlation of this composite unit across the map area. This unit occurs in a locally low stratigraphic position, but this does not infer correlation across the map area or elsewhere.
st	**shield terrain**	Medium- to low-radar-backscatter material of heterogeneous texture; composed of distributed edifices and associated material that forms a locally thin layer; shield edifices marked by high- or low-backscatter, with or without distinct edifices. See Hansen (2005) for a more complete description of the nature of this terrain type.	Composite shield-related volcanic materials. Given the potential time-transgressive nature, this is a lithodemic unit.	This is a descriptive unit with no implication for temporal relations across the map area. Deformed by suites of variably preserved/developed lineament trends and by regional wrinkle ridges.
btu	**basal terrain, undivided**	High- to low-radar-backscatter materials, can include shields (generally less than 5 km diameter); composite unit that marks a local basal terrain.	Basal material of unknown age and most certainly represents a range of ages of formation across the map area. Given the potential time-transgressive nature, this is a lithodemic unit.	This is a descriptive unit with no implication for temporal relations across the map area. Deformed by suites of variably preserved/developed lineament trends and by regional wrinkle ridges.
btAk	**Akhtamar Planitia basal terrain**	Medium-radar-backscatter materials; scattered small shield volcanoes; preserved in NE-trending broad topographic ridges in the vicinity of Tellus Regio.	Basal material of volcanic origin that locally postdated ribbon-tessera terrain and predated adjacent plains material.	Near Tellus Regio unit is cut by regional NE-trending folds and ridges and NE-trending fractures; in Akhtamar Planitia unit occurs in NW-trending broad topographic ridges and cut by NE-trending folds and fractures. Locally deformation overprints the primary textural characteristics of the materials.
btVA	**Atalanta/Vellamo planitiae basal terrain**	Medium-radar-backscatter materials; outcrops in broad NNE-trending topographic ridges	Basal material of volcanic origin that locally postdate ribbon-tessera terrain and predate plains material.	Deformed by NNE-trending medium wavelength folds and ridges, and local fractures orthogonal to the folds and regional NNE-trending fractures and graben. Deformation structures do not completely obscure the characteristics of the basal volcanic materials.
btL	**Leda/Lowana planitiae basal terrain**	Medium-radar-backscatter materials; scattered small shield volcanoes. Locally where unit is in contact with shield terrain contacts are gradational; shields occur in both units; composite unit that marks a local basal terrain.	Basal material of unknown age and most certainly represents a range of ages of formation across the map area. Given the potential time-transgressive nature, this is a lithodemic unit.	This is a descriptive unit with no implication for temporal relations across the map area. Deformed by suites of variably preserved/developed lineament trends and by regional wrinkle ridges.
btLl	**Llorona Planitia basal terrain**	Medium-radar-backscatter materials; scattered small shield volcanoes	Basal material of volcanic origin that locally postdate ribbon tessera terrain and predate plains material.	Deformed by NW-trending folds and NE-trending fractures. Local NW-fractures impart a reticulate appearance. Deformation structures does not completely obscure the characteristics of the basal volcanic materials.
		RIBBON TESSERA TERRAIN AND RELATED MATERIAL		
fibu	**intratessera basin flow material, undivided**	Low- to medium-radar-backscatter materials, locally embays small troughs and ridges and narrow to broad intratessera topographic basins; may contains numerous shields.	Low-viscosity flows emanating from local sources within structural lows in ribbon-tessera terrain of host crustal plateaus; material floods preexisting ribbons and folds, and is affected by later-formed ribbon-tessera terrain structures. Intratessera volcanism played an important role in ribbon-tessera terrain formation and in crustal plateau evolution (Hansen and others, 1999; Banks and Hansen, 2000; Hansen, 2006). Specific ifb units are delineated by spatial location across the map area (i.e., host ribbon-tessera terrain).	Intratessera volcanism plays and important role in ribbon-tessera formation and in crustal plateau evolution (Hansen and others, 1999; Banks and Hansen, 2000). These are descriptive units with no temporal implications across the map area. Unit ifb forms throughout the tectonic evolution of host ribbon-tessera terrain (Hansen, 2006).
fibM	**intratessera basin flow material of Manatum Tessera**	Low- to medium-radar-backscatter material filling lows in rtM.	Low-viscosity flows emanating from localized sources within structural lows in ribbon tessera terrain of Manatum Tessera, western Ovda Regio; material floods preexisting ribbons and folds, and is affected by later-formed ribbon-tessera terrain structures.	These are descriptive units with no temporal implications across the map area. Unit ibM forms throughout the tectonic evolution of host ribbon-tessera terrain (Hansen, 2006).
fibO	**intratessera basin flow material of Ovda Regio**	Low- to medium-radar-backscatter material filling lows in rtO.	Low-viscosity flows emanating from localized sources within structural lows in ribbon tessera terrain of Ovda Regio; material floods preexisting ribbons and folds, and is affected by later-formed ribbon-tessera terrain structures.	These are descriptive units with no temporal implications across the map area. Unit ibO forms throughout the tectonic evolution of host ribbon-tessera terrain (Hansen, 2006). This unit is the same that materials under the same denomination in the Aphrodite Map Area (Hansen and López, 2020) and correlative with ibO in V-23 (Hansen, 2009) and with ifb in V-35 (Bleamaster and Hansen, 2005).
fibT	**intratessera basin flow material of Tellus Tessera**	Low- to medium-radar-backscatter material filling lows in rtT.	Low-viscosity flows emanating from localized sources within structural lows in ribbon tessera terrain of Tellus Tessera; material floods preexisting ribbons and folds, and is affected by later-formed ribbon-tessera terrain structures.	These are descriptive units with no temporal implications across the map area. Unit ibM forms throughout the tectonic evolution of host ribbon-tessera terrain (Hansen, 2006).
rt	**ribbon tessera terrain undivided**	High-radar-backscatter material, marked by suites of extensional (ribbons and graben) and contractional (short- to long-wavelength folds) structures.	Extensively deformed ribbon and fold structures and patterns similar to extended ribbon-fold terrain (Hansen and Willis, 1996, 1998) and to the marginal fold belt domain of crustal plateaus (Ghent and Hansen, 1999) and lowland ribbon-tessera terrain inliers (Hansen, 2006).	Specific rt units represent lithodemic terrain with similar deformation and topography. No evidence indicates that rt units formed synchronously, although rt units reflect unique formation conditions (Hansen and Willis, 1996; Hansen, 2006). This is a descriptive unit with no temporal implications across the map area.
rtMe	**Meni ribbon-tessera terrain**	High-radar-backscatter material, marked by suites of extensional (ribbons and graben) and contractional (short- to long-wavelength folds) structures.	Extensively deformed ribbon and fold structures and patterns similar to extended ribbon-fold terrain (Hansen and Willis, 1996, 1998) and lowland ribbon-tessera terrain inliers (Hansen, 2006).	This is a descriptive unit with no temporal implications across the map area.
rtDe	**Dekla ribbon-tessera terrain**	High-radar-backscatter material, marked by suites of extensional (ribbons and graben) and contractional (short- to long-wavelength folds) structures.	Extensively deformed ribbon and fold structures and patterns similar to extended ribbon-fold terrain (Hansen and Willis, 1996, 1998) and to the marginal fold belt domain of crustal plateaus (Ghent and Hansen, 1999) and lowland ribbon-tessera terrain inliers (Hansen, 2006).	
rtT	**Tellus Regio ribbon-tessera terrain**	High-radar-backscatter material, generally occurs at moderate-high topography (~2-4 km above MPR), marked by suites of extensional (ribbons and graben) and contractional (short- to long-wavelength folds) structures.	Material of unknown genetic origin deformed into coherent identifiable masses by the process of crustal plateau formation (Hansen and Willis, 1998; Ghent and Hansen, 1999; Hansen, 2006).	
rtAn	**Ananke ribbon-tessera terrain**	High-radar-backscatter material, marked by suites of extensional (ribbons and graben) and contractional (short- to long-wavelength folds) structures.		
rtNe	**Nemesis ribbon-tessera terrain**	High-radar-backscatter material, marked by suites of extensional (ribbons and graben) and contractional (short- to long-wavelength folds) structures.		
rtAt	**Athena ribbon-tessera terrain**	High-radar-backscatter material, marked by suites of extensional (ribbons and graben) and contractional (short- to long-wavelength folds) structures.		
rtLi	**Likho ribbon-tessera terrain**	High-radar-backscatter material, marked by suites of extensional (ribbons and graben) and contractional (short- to long-wavelength folds) structures.		This is a descriptive unit with no temporal implications across the map area.
rtKu	**Kutue ribbon-tessera terrain**	High-radar-backscatter material, marked by suites of extensional (ribbons and graben) and contractional (short- to long-wavelength folds) structures.		
rtSh	**Shimti ribbon-tessera terrain**	High-radar-backscatter material, marked by suites of extensional (ribbons and graben) and contractional (short- to long-wavelength folds) structures.		
rtGe	**Gegute ribbon-tessera terrain**	High-radar-backscatter material, marked by suites of extensional (ribbons and graben) and contractional (short- to long-wavelength folds) structures.		
rtHb	**Hasetsse-baad ribbon-tessera terrain**	High-radar-backscatter material, marked by suites of extensional (ribbons and graben) and contractional (short- to long-wavelength folds) structures.		
rtO	**Ovda Regio ribbon-tessera terrain**	High-radar-backscatter material, generally occurs at high topography (~3-5 km), marked by suites of extensional (ribbons and graben) and contractional (short- to long-wavelength folds) structures. Geographically located in eastern Ovda Regio.	Material of unknown genetic origin deformed into coherent identifiable masses by the process of crustal plateau formation (Hansen and Willis, 1998; Ghent and Hansen, 1999; Hansen, 2006).	
rtM	**Manatum ribbon-tessera terrain**	High-radar-backscatter material, generally occurs at moderate topography (~2 km), marked by suites of extensional (ribbons and graben) and contractional (short- to long-wavelength folds) structures.	Material of unknown genetic origin deformed into coherent identifiable masses by the process of crustal plateau formation (Hansen and Willis, 1998; Ghent and Hansen, 1999; Hansen, 2006).	

Plate 1. *(Continued)*

materials including basal-shield transitional terrain and shield terrain (Aubele, 1996; Hansen, 2005), local volcano- and corona-related flow materials, and undivided volcanic materials; and (e) 146 impact craters.

4.1. Primary Structures, Secondary Structures, and Tectonic Fabrics

Different structures, both primary (depositional or emplacement-related) and secondary (tectonic), are identified in NASA Magellan SAR data. Tectonic fabrics represent suites of structures that together define a coherent structural pattern or fabric and that may be genetically related.

4.1.1. Primary Structures

Primary structures are mostly related to volcanic and impact processes and include features such as channels, shields, pits/pit chains, lobate flow fronts and flow levees, and crater rims and impact-related haloes and splotches (Ford et al., 1993).

Channels or canali are sinuous, low-backscatter troughs tens to thousands of kilometers long and a few kilometers wide; locally, they may lack apparent topographic relief; they are similar to terrestrial fluvial channels, interpreted to form by channelized fluid flow (Baker et al., 1992, 1997; Komatsu & Baker, 1994). A large section of Baltis Vallis, the longest channel on Venus (~6,800 km), transects Atalanta Planitia in eastern NMA. Both the nature of the fluid and formational mechanism (constructive or erosional) are unknown (e.g., Bussey et al., 1995; Gregg & Greely, 1993; Jones & Pickering, 2003; Lang & Hansen, 2006; Waltham et al., 2008; Williams-Jones et al., 1998). Canali could be primary constructional structures, related to levee development during flow emplacement, secondary erosional structures that cut earlier emplaced material, or a combination of both.

Shields, interpreted as small volcanic edifices, are small (generally 1 to 15 km in diameter, rarely 20 km in diameter), quasi-circular to circular, radar-dark or radar-bright features with or without topographic expression and with or without a central pit (Addington, 2001; Crumpler et al., 1997; Guest et al., 1992). The size of individual shields is difficult to constrain because bases of individual shields are typically poorly defined, and deposits commonly blend smoothly into a composite layer that cannot be treated as a time line or marker unit with any certainty (Hansen, 2005).

Intermediate volcanoes, such as steep-sided domes or tholi, represent volcanic features indicative of a higher viscosity either due to a more felsic composition and/or differences in the texture or rate of the extruded magma (e.g., Pavri et al., 1992; Stofan et al., 2000).

Lobate flow fronts and flow levees developed within flow units can indicate surface flow direction, which in turn can provide information about flow emplacement and local topography at the time of flow emplacement.

Impact craters are perhaps most prominently marked by rims that sit above circular interiors and within/at the boundary of ejecta material marked by extremely radar-bright deposits (Weitz, 1993). Some impact craters display haloes, radar-bright (rough), or radar-dark (smooth) deposits that extend outward from the rim and ejecta deposits up to many crater diameters (Izenberg et al., 1994). Haloes are thought to form as a result of the shock-induced crushing of host material just preceding or accompanying bolide impact or due to accumulation of fine-scale ejecta. Some craters have parabolic haloes that extend up to 20 crater radii to the west; these thin deposits are interpreted as due to the interaction of east-to-west zonal winds (Arvidson et al., 1991; Campbell et al., 1992, 2015; Schaller & Melosh, 1998; Whitten & Campbell, 2016). Numerous dark splotches also occur within the map area; these could represent bolides that exploded before impact (Kirk & Chadwick, 1994).

Crater haloes, parabolic deposits, and dark splotches appear to degrade with time resulting in a decrease in radar contrast relative to surrounding terrain (Izenberg et al., 1994). Impact craters that display both extreme haloes and radar-bright crater interiors are generally interpreted as relatively young, whereas craters with degraded haloes, or lacking haloes entirely, and displaying radar-smooth filled interiors are interpreted as relatively old (Herrick & Rumpf, 2011; Phillips & Izenberg, 1995). Impact crater haloes and dark splotches are indicated with a transparent map pattern so that underlying units and structures can be represented along with the extent of crater haloes.

4.1.2. Secondary Structures

Secondary structures or tectonic structures form after the emplacement of geologic units and typically record tectonic processes. In addition, the distribution and (or) character of secondary structures may provide clues for the delineation of material units, as well as temporal relations between different material units (Hansen, 2000). Secondary structures within NMA include various types of lineaments: (a) fractures and faults; and (b) broad ridges, folds, and wrinkle ridges. Given that the map area covers ~60,000,000 km^2 we cannot and do not show all lineaments. The focus here is an attempt to capture the essence of recognized structural suites. Therefore, in some cases lineament trends will be shown; in other cases each lineament is shown, in yet other cases a collection of the lineaments is shown. There is no single unique scale of lineament or feature identification, just as there is no single unique scale of observation in the case of field-based mapping on Earth, particularly for maps that cover huge areas of Earth's surface.

Fractures are sharply defined lineaments with a negative, or null, topographic signature, commonly grouped into suites based on orientation, pattern (i.e., parallel or near parallel, radial, or concentric) and/or spacing (i.e., widely spaced or closely spaced). Fractures are generally interpreted as extensional structures (Banerdt et al., 1997). In some cases fractures appear as sets of paired lineaments and may mark graben. Locally fractures consist of *en echelon* fractures indicative of either a shear fracture origin or the emergence of a fracture at depth to the surface with the *en echelon* fractures marking hackles.

Some fractures in local radial suites transition to pits or pit chains, or sharply defined depressions. Linear arrays of pits likely represent regions marked by subsurface excavation; they may mark the surface expression of dilatational faults or dikes (Bleamaster & Hansen, 2005; Ernst et al., 2003; Ferrill et al., 2004; Grosfils & Head, 1994; Okubo & Martel, 1998; Schultz et al., 2004), or they could represent stoping features that would not require associated crustal extension (e.g., Cushing et al., 2015). Pits or pit chains can be considered primary structures or secondary structures, depending on the question at hand; pits are primary structures relative to pit-related materials, yet they may be secondary structures relative to the units they cut or are emplaced within.

Folds are ridges with a gradational radar character normal to their trend and wave-like topographic expression; they are generally interpreted as contractional structures (Stofan et al., 1993). Small ridges are topographic ridges with low relief and width, similar in appearance to folds except that the nature of the lineaments is ambiguous—though possibly of contractional origin (marked by folds or thrust faults).

Wrinkle ridges define low sinuous structures spaced a few kilometers to tens of kilometers apart and up to a few hundred kilometers long. These lineaments, which represent low values of layer contractional strain (<2%), are found on most terrestrial worlds, especially on large flat expanses of volcanic flow materials (Banerdt et al., 1997; Watters, 1988). Locally wrinkle ridges occur as inversion structures formed by the inversion of fracture-fill material due to post burial contraction (DeShon et al., 2000). Wrinkle ridges typically form suites of near parallel structures (and occasionally orthogonal suites) formed over large regional expanses.

4.1.3. Tectonic Fabrics

Tectonic fabrics are an assemblage of related structural elements that together characterize a rock unit, as in the case of ribbon-tessera terrain (Hansen, 2006; Hansen & Willis, 1996, 1998).

Ribbon-tessera fabric is characterized by orthogonally developed suites of ribbons, or ribbon structures and folds. For a complete description of this tectonic fabric and its implications on the origin and evolution of tessera-terrain and crustal plateaus see Hansen and Willis (1996, 1998), Ghent and Hansen (1999), Brown and Grimm (1999), Hansen (2006), and Ruiz (2007). For a discussion of ribbon-terrain controversies, see Gilmore et al. (1998), Hansen et al. (2000), Hansen (2006), and Hanmer (2020).

Within the NMA we delineate ribbon-tessera ribbon and fold trends. Ribbon structures are shown as trends of ribbon ridges and troughs; fold structures demarcate fold crest or trough trends. In most cases short-, intermediate-, and long-wavelength folds define locally parallel trends (Hansen, 2006). Graben complexes, common elements of ribbon-tessera terrain fabric, typically parallel ribbon trends. Graben complexes can be differentiated from ribbons on the basis of smaller length-to-width ratios—that is, graben complexes are generally wider and shorter than ribbon structures. Ribbon-tessera graben complexes typically cut at high angles to long-wavelength fold crests, commonly resulting in a lens-shape plan view. Some graben complexes define broad patterns (radial and concentric) that could offer information on the evolution of the crustal plateaus after and during the formation of the ribbon-tessera fabric. Bindschadler et al. (1992) recognized ribbon, fold, and graben structures within tessera terrain. These workers describe ribbon structures as "narrow troughs," clearly differentiating ribbon structures from generally parallel but morphologically different graben complexes.

4.2. Map Units

Map units interpreted across the NMA are broadly defined in this section. The map legend provides a complete description of units.

The contacts between adjacent units vary from well-defined whereas in other cases are approximate or gradational, due to the angular nature of individual contacts or the style of the units or terrains. For example, shield terrain (unit st) consists of a thin veil of numerous in situ locally sourced deposits associated with individual shields, typically on the order of a few km or less across (Guest et al., 1992; Hansen, 2005); the location of the mapped contact could vary across tens and locally perhaps even hundreds of kilometers given the inherent challenges in recognizing individual shields and the wide variation in shield density (e.g., Hansen, 2009; Hansen & Tharalson, 2014). In the case of some basal terrains that were cut by fractures following host unit formation, and later locally buried by younger material, the contact between the basal terrain and younger units can be sharp, marked by fracture truncation. The contacts can also be gradational wherein the fractures are visible yet do not obviously cut the overlying material. In this case the overlying material is interpreted to form a thin layer that buries earlier formed buried fractures. The transition from a gradational to sharp contact can itself be very sharp or gradational. In addition, the amount/character of fracture burial can also be gradational.

4.2.1. Terrain Units

The term "terrain" describes a texturally defined region, for example, where tectonism imparted a surface with a penetrative deformation that disallows interpretation of the original unit or units (Wilhelms, 1990). The characteristic texture of a terrain could imply a shared history, such as a terrestrial tectono-thermal history or an event that melds possibly previously unrelated rock units (any combination of igneous, metamorphic, and sedimentary rocks); no unique history is inferred or required prior to the event(s) that melded potentially separate units into the textural terrain (i.e., lithodemic unit). Events prior to terrain formation are unconstrained in time or process unless specifically noted. Three general classes of terrain units occur across NMA: ribbon-tessera terrain and associated units, basal terrain, and shield terrain and associated basal-shield transitional terrain.

4.2.1.1. Ribbon-Tessera Terrain and Associated Units

Ribbon-tessera terrain and associated intratessera basin units are widespread across the NMA marking the characteristic surface of crustal plateaus (Western Ovda/Manatun Tessera, and Ovda, Thetis, and Tellus Regiones) and also occurring as lowland inliers. Units include the descriptive moniker plus the name of the host tessera region (e.g., Ovda or Tellus ribbon tessera terrain, rtO and rtT, respectively; or itbO and itbT). A descriptive term such as undivided (rtu) is applied to the relatively small exposures located in unnamed locations. Ribbon-tessera terrain exposures are typically characterized by orthogonal ribbon-fold tessera fabric (Hansen, 2006; Hansen & Willis, 1998). Fold wavelengths range from less than 1 km—essentially to the effective resolution of SAR data, to tens of kilometers. Ribbon wavelengths range from 2 to 5 km, and below, locally also to SAR effective resolution. Orthogonal ribbon-fold fabrics are the most common tessera fabric across NMA as they are for ribbon-tessera terrain globally (Hansen & López, 2010), but local shear fabrics (Hansen, 1992; Hansen & Willis, 1996) occur in central Ovda Regio and in tessera inliers in Niobe Planitia (e.g., Shimti-Kutue Tesserae). Intratessera basin material, which typically fills short- to long-wavelength tessera-fold troughs (short-wavelength fold troughs are below the scale of the NMA), is best preserved and identified within crustal plateaus, although we delineate such units within large tesserae inliers. Tesserae inliers describe regional-scale linear to arcuate patterns in lowland basins. Given that inliers reside at low elevation and are locally embayed by younger volcanic materials, unique identification of intra-tessera basin material (as opposed to undivided volcanic material) can be difficult. For a more complete description of intra-tessera basin materials or the origin of crustal plateaus see Banks and Hansen (2000) and Hansen (2006).

4.2.1.2. Local Basal Terrain

Local basal terrain is a term used to describe surfaces that lie within locally low stratigraphic positions relative to adjacent map units in planitiae. Similar to the naming scheme used in other terrain units we include the moniker basal terrain, and the name of the host planitia (e.g., Niobe or Leda basal terrain, btNi and btLe,

10.1029/2020EA001171

Table 1
Niobe Region (I-2467) Impact Craters

Name	Latitude (°N)[a]	Longitude (°E)[a]	Diameter (km)[a]	Elevation[a]	Vmap	Units	Ejecta blanket[a]	Impact halo (km)[a]	Central Peak[a]	Rim[a]	Dark Floor[a]	Crater density[a]	Crater database	Deformed[a]	Temporal implications
Adivar	8.9	76.2	29	6,051.76	22	vmu	Y	70	Y	Y	Y	2.55	H,S?	N	Postdates ACWR formation
Adzoba	12.8	117	12.2	6,051.50	23	bst	Y	x	N	Y	N	3.18	H,S	N	Postdates ARF and AWCR formation
Afua	15.5	124	11	6,051.45	24	btL, bst	Y	x	N	Y	N	3.18	H,S	Y	
Aimee	16.1	127.2	16.8	6,051.09	24	fcA	Y	50	Y?	Y	N	2.86	H,S	N	Postdates ACWR formation
Almeida	46.6	123.3	14.9	6,051.92	12	st	Y	140	Y	Y	N	2.86	H,S	N	Postdates ARF formation
Altana[b]	1.5	69.9	5.7	6,053.47	22	rtMa, fcK	Y	x	N	Y	N	2.23	H	N	
Amaya	11.3	89.3	34	6,052.56	22	bst, fcOv	Y	120	Y	Y	Y	2.55	H,S	N	Postdates ARF and local radial fractures, with possible later structural reactivation
Anaxandra	44.2	162.3	20.2	6,051.31	13	vmu	Y	80	Y	Y	Y	1.59	H,S	N	Postdates ARF, ARF burial and subsequent inversion, and ACWR
Antonina	28.1	106.9	11	6,050.63	11	vmu	N	60	N	N	N	2.23	H,S	N	Postdates ACWR formation
Anush	14.9	86.5	12.2	6,051.88	22	bst	Y	x	Y	Y	Y	1.91	H,S	N	Postdates ACWR formation
Asmik	3.9	166.5	18.6	6,051.57	25	fcRu2	Y	130	N	Y	Y?	3.5	H,S	N	Postdates ARF, ARF burial and subsequent inversion, and ACWR formation
Avene	40.4	149.4	11	6,051.08	13	vmu	Y	40	N	Y	N	2.55	H,S	N	Postdates ACWR formation
Ban Zhao	17.2	146.9	38.3	6,050.80	24	vmu, btL	Y	x	Y	Y	N	2.86	H,S	N	Postdates ACWR formation
Barrera	16.5	109.4	26.8	6,051.67	23	bst, st	Y	70	Y	Y	Y	3.18	H,S	N	Postdates ACWR formation
Barto	45.3	146.2	47.9	6,051.30	12	vmu	Y	x	Y	Y	Y	3.82	H,S	N	Postdates ACWR formation?
Bernhardt	31.6	84.4	25	6,052.02	10	bst	Y	x	Y	Y	Y	2.55	H	N	
Bourke-White	21.2	147.9	34.4	6,050.96	24	vmu	Y	120	Y	Y	Y	2.55	H,S	N	Postdates ACWR formation
Budevska	0.5	143.2	18.7	6,052.22	24	st	Y	70	Y	Y	N	2.55	H,S	N	Postdates ARF formation
Caccini	17.4	170.4	37.5	6,051.68	25	vmu	Y	130	Y	Y	N	1.91	H,S	N	Postdates ACWR formation
Caldwell	23.6	112.5	52	6,051.52	23	bst	Y	x	Y?	Y	N	3.18	H,S	N	Postdates ACWR formation
Callirhoe	21.2	140.7	32.9	6,051.33	24	st	Y	x	Y	Y	Y	2.55	H,S	N	Postdates NW-fracture formation, although NW-fractures may show local evidence of later reactivation

10.1029/2020EA001171

Table 1
Continued

Name	Latitude (°N)[a]	Longitude (°E)[a]	Diameter (km)[a]	Elevation[a]	Vmap	Units	Ejecta blanket[a]	Impact halo (km)[a]	Central Peak[a]	Rim[a]	Dark Floor[a]	Crater density[a]	Crater database	Deformed[a]	Temporal implications
Carter	5.3	67.3	19.3	6,054.13	22	rtMa	Y	55	N	Y	N	2.23	H,S	N	
Cather	47.1	107	26.5	6,051.60	11	st?	Y?	x	N	Y	Y	1.27	H,S	N	
Chapelle	6.4	103.8	20.8	6,051.86	23	fcOv	Y	x	Y	Y	Y	2.23	S	N	
Christie	28.3	72.7	24.3	6,050.84	10	vmu	Y	170	Y	Y	Y	2.55	H,S	N	Postdates ACWR formation
Cochran	51.9	143.4	98.1	6,051.77	4	vmu	Y	x	N	Y	Y	3.18	H,S	N	Postdates ACWR formation
Cori	25.4	72.9	54.7	6,050.79	10	vmu	Y	x	N	Y	Y	2.86	H,S	N	Postdates ACWR formation
Corpman	0.3	151.8	45.1	6,052.21	25	fcOv	Y	110	N	Y	Y	3.5	H,S	N	Postdates ARF formation, although ARF may also been locally reactivated
Datsolalee	38.3	171.8	17	6,051.44	13	bst	Y	120	N	Y	N	1.27	H,S	Y?	
de Beauvoir	2	96.1	53.3	6,054.79	23	rtO, itbO	Y	x	N	Y	Y	3.82	H,S	N	
Doris	2.3	90	15.5	6,055.01	22.23	rtO	Y?	x	N	Y	Y	0	H,S	Y	Predates ARF or local radial fractures
du Chatelet	21.5	165	19	6,051.73	25	vmu	Y	60	?	Y	?	1.91	H,S	N	Big enough to show?
Erkeley	43.9	103.4	9.3	6,051.69	11	vmu	N	x	N	N	N	1.27	H,S	N	
Escoda	18.2	149.5	19.5	6,051.12	24	vmu, fcI	Y	x	N	Y	Y	2.23	H,S	N	Postdates ACWR formation
Estelle	1.1	93.7	17.8	6,055.06	23	rtO, itbO	Y?	x	Y	Y	N	3.5	H,S	N	
Faiga	4.9	170.9	10.6	6,051.48	25	fcRu2	Y	70	N	Y	N	3.5	H,S	N	
Fazu	32.4	106	7.1	6,050.75	11	vmu	Y	60	N	Y	N	1.91	H,S	N	
Ferrier	15.7	111.3	29	6,051.51	23	bst	Y	x	Y	Y	Y	3.18	H,S	N	Crater may postdate ARF formation, but ARF may have been locally reactivated after crater formation
Fiona	5	166.6	5	6,051.40	25	fcRu2	Y	30	N	Y	N	3.5	H,S	N	
Firuza	51.8	108	4.9	6,051.50	3	bst	Y	x	N	Y	N	0	H,S	N	
Frosya	29.5	113.4	9.6	6,050.87	11	vmu	Y	50	N	Y	N	3.5	H,S	N	Postdates ACWR formation
Greenaway	22.9	145.1	92.3	6,051.28	24	btLl, st, vmu	Y	x	N	Y	N	2.55	H,S	N	Postdates ACWR formation
Gregory	7.1	95.8	18	6,053.17	23	bst	Y	x	N	Y	N	3.18	H,S	N	Postdates ARF formation
Hannah	17.9	102.6	19.1	6,051.54	23	st	Y	x	Y	Y	Y?	2.55	H,S	N	Postdates ACWR formation
Helvi	12.4	82.7	11.2	6,052.35	22	bst	Y	x	N	Y	N	2.55	H,S	N	Postdates ARF formation
Hepworth	5.1	94.6	62.5	6,054.16	23	rtO, itbu	Y	x	N	Y	Y	3.5	H,S	N	
Himiko	19	124.3	36.7	6,051.42	24	fcA, bst	Y	x	Y	Y	N	2.86	H,S	N	Postdates ARF and AWCR formation, and formation of

Table 1
Continued

Name	Latitude (°N)[a]	Longitude (°E)[a]	Diameter (km)[a]	Elevation[a]	Vmap	Units	Ejecta blanket[a]	Impact halo (km)[a]	Central Peak[a]	Rim[a]	Dark Floor[a]	Crater density[a]	Crater database	Deformed[a]	Temporal implications
															concentric fractures of Abundia Corona and the steep sided dome
Horner	23.4	97.8	24.7	6,051.36	23	bst, fcOv	Y	x	Y	Y	Y	2.86	H,S	N	Postdates formation of concentric fractures of Maya Corona
Hwangcini	6.3	141.7	30.8	6,051.73	24	st	Y	230	Y	Y	Y	2.55	H,S	N	Postdates ARF formation
Icheko[b]	6.6	97.9	5.6	6,053.53	23	bst	Y	x	N	Y	N	2.86	H,S	N	Postdates tessera ribbon fabric formation, but may be deformed by reactivation of ribbon structures?
Iraida[b]	27.8	108	6	6,050.65	11	vmu	Y	x	N	Y	N	1.91	H	N	Postdates ARF, ARF burial and subsequent inversion as WRs
Irene	49.8	134	13.5	6,052.15	12	rtA, st	Y	x	N	Y	N	4.14	H,S	Y?	
Irina	34.9	91.2	14.2	6,051.47	11	st	Y	x	N	Y	Y	1.59	H,S	N	Postdates ACWR formation
Irinuca[b]	51.4	121.9	8.1	6,051.80		fmJ	Y	x	N	Y	N	2.23	H,S	N	
Jaantje	46.5	123.1	7.3	6,051.98		st	Y	140	N	Y	N	2.86	H,S	N	Postdates ARF formation
Jamila	45.8	134.7	7.8	6,051.72	12	vmu	Y	50	N	Y	N	3.5	H,S	N	Postdates ACWR formation
Khadako	54.2	139.4	7	6,051.95	4	itbu	Y?	x	N	Y	Y	2.86	H,S	Y?	Posts formation or reactivation of NE and NW-trending fractures
Khatun	40.3	87.2	42.4	6,052.55	10	rtT	Y	120	Y	Y	Y	1.27	H,S	N	
Kiris	20.9	98.8	13.3	6,051.67	23	bst	Y	x	N	Y	N	2.23	H,S	N	Postdates formation of NW-trending fractures and ARF, but these fracture suites may have been reactivated after crater formation
Kollwitz	25.2	133.6	28.9	6,051.23	12	btLl, bst, vmu	Y	x	Y	Y	Y	1.27	H,S	N	
Konopnicka	14.5	166.6	19.9	6,051.74	25	vmu	Y	60	Y	Y	Y	2.55	H,S	N	
Kylii	41.1	67	12.8	6,051.46	10	bst	Y	x	Y	Y	N	1.59	H,S	N	
Laura	48.9	141.2	18.4	6,051.46	12	vmu	Y	x	N	Y	N	3.82	H,S	N	Temporal relations between crater and WRs unclear due to spacing of wrinkle ridges, low strain, and radar brightness of both ejecta and WRs
	23.7	94.6	22.4		23	bst		x	Y	Y	N	2.55	H,S	N	

Table 1
Continued

Name	Latitude (°N)[a]	Longitude (°E)[a]	Diameter (km)[a]	Elevation[a]	Vmap	Units	Ejecta blanket[a]	Impact halo (km)[a]	Central Peak[a]	Rim[a]	Dark Floor[a]	Crater density[a]	Crater database	Deformed[a]	Temporal implications
Li Quingzhao															Crater postdates formation of NW-trending fractures
Lullin	23	81.3	24.9	6,051.80	22	bst, fcKu2	Y	160	Y	Y	Y	2.86	H,S	N	Postdates ACWR formation
MacDonald	30	120.7	18.4	6,051.70	12	st	Y	90	N	1	Y?	1.59	H,S	N	Postdates ACWR formation
Manzolini	25.7	91.3	43.7	6,051.67	11	bst, st	Y	x	Y	Y	Y	2.55	H,S	N	Predates ARF
Maranda	4.9	169.7	17.1	6,051.53	25	fcRu2	Y	x	Y	Y	Y?	3.5	H,S	Y?	Predate local radial fractures
Marere[b]	19.6	65.8	6.7	6,051.15	22	vmu	Y	x	N	Y	N	2.23	H,S	N	
Maria Celeste	23.4	140.4	96.6	6,051.38	24	vmu, st	Y	x	N	Y	Y	2.86	H,S	N	Temporal relations with WRs difficult to robustly constrain given the presence of extensive halo deposits
Marysya[b]	53.3	75.1	6.9	6,051.39	3	btu	Y?	x	N	Y	N	1.91	H,S	Y	
Mbul'di[b]	23.8	74.7	5.5	6,050.73	22	vmu	Y	x	N	Y	N	2.86	H,S	N	Postdates ACWR formation
Merian	34.5	76.2	21.9	6,052.88	10	rtT	Y?	x	?	Y	N	1.59	H,S	Y	
Merit Ptah	11.4	115.6	17	6,051.19	23	bst	N	x	N	N	N	2.86	H,S	N	Postdates formation of NW-trending fractures at this location
Millay	24.4	111.3	48.3	6,051.33	23	bst	Y	x	Y	Y	Y	2.86	H,S	N	Postdates ACWR formation
Mosaido	17.3	75.2	7.3	6,051.59	22	bst	Y	x	N	Y	N	3.5	H,S	N	Postdates ACWR formation
Moses	34.6	119.9	28.1	6,051.09	11	bst, st	Y	x	Y	Y	Y	2.23	H,S	N	Postdates ACWR formation
Mu Guiying	41.2	81.1	32.7	6,051.60	10	bst	Y	x	Y	Y	N	1.59	H,S	N	
Nana	49.8	75.4	8.3	6,051.35	10	st	Y	x	N	Y	N	1.59	H,S	N	
Naomi	6	70.3	17.1	6,053.07	22	rtMa, bst	Y?	x	N	Y	N	2.55	H,S	Y	Predates formation of radial fractures associated with Kaltash Corona?
Neeltje	12.4	124.5	10.3	6,051.27	24	btL	N	x	?	Y	?	4.14	H,S	N	
Nemcova	5.9	125.1	21.4	6,052.47	24	fcRo	Y	90	Y	Y	Y	1.91	H,S	N	Postdate formation of radial fractures associated with Rosmerta Corona
Nijinskaya	25.8	122.5	35.4	6,051.09		vmu, bst	Y	x	Y	Y	Y	2.55	H,S	N	
Nsele[b]	6.7	64.2	4.9	6,053.50	22	vmu	Y?	40	N	Y	N	2.23	H,S	N	
Nyal'ga[b]	17	64.5	5.2	6,051.49	22	vmu	Y?	x	N	Y	N	1.59	H,S	N	
Odarka	40.7	138.2	7.2	6,051.6	12	vmu	Y	70	N	Y	N	2.55	H,S	N	Postdates ACWR formation

10.1029/2020EA001171

Table 1
Continued

Name	Latitude (°N)[a]	Longitude (°E)[a]	Diameter (km)[a]	Elevation[a]	Vmap	Units	Ejecta blanket[a]	Impact halo (km)[a]	Central Peak[a]	Rim[a]	Dark Floor[a]	Crater density[a]	Crater database	Deformed[a]	Temporal implications
Ogulbek[b]	2.4	145.1	6.6	6,052.29	24	bst	Y?	70	N	Y	N	2.86	H	N	Postdates formation of ARF
Olena[b]	10.9	149	7	6,051.42	22	bst	Y	x	N	Y	N	2.55	H,S	N	Postdates formation of local WR formation
Ortensia	7.6	155.7	6.6	6,051.78	25	fsL	Y	50	N	Y	N	1.91	H,S	N	
Oshalche	29.7	155.5	9.6	6,050.91	13	vmu	Y	x	N	Y	Y?	0.64	H,S	N	
Parra	20.5	78.5	42.8	6,052.02	22	fcKu2	Y	140	N	Y	N	3.5	H,S	N	
Pasha	42.7	156.3	7.6	6,050.66		vmu	Y	50	N	Y	N	2.55	H,S	N	Postdates ACWR formation
Phyllis	12.2	132.4	10.6	6,051.74	24	bst, st	Y	130	N	Y	N	2.55	H,S	N	Postdates ARF formation
Polina	42.4	148.2	20.5	6,051.18	11	vmu	Y	130	N	Y	N	2.86	H,S	N	
Puhioia[b]	20.6	69.4	6.4	6,051.02	22	vmu	Y?	x	N	Y	N	0	H,S	N	
Qulzhan	23.5	165.4	10.8	6,051.33	25	vmu	Y	140	N	Y	N	1.59	H,S	N	Postdates ACWR formation
Quslu	6.2	166.8	8.6	6,051.34	25	fcRU2	Y	x	Y	Y	N	3.18	H,S	N	Postdates formation of ARF and ACWR
Rampyari	50.6	179.3	6	6,050.75	4	vmu	Y	80	N	Y	Y	2.23	H	N	Postdates ACWR formation
Regina	30	147.3	25.5	6,051.35	12	bst	Y	220	Y	Y	Y	1.59	H,S	N	
Riley	14	72.5	18.8	6,051.91	22	fmU1	Y	80	Y	Y	Y?	2.86	H,S	N	
Romanskaya	23.2	178.5	31.7	6,052.18	25	fRk	Y	80	Y?	Y	Y	0.95	H,S	Y	
Rowena	10.4	171.4	19.6	6,051.48	25	fcRu2	Y	x	Y	Y	Y	3.82	H,S	N	Postdates WR formation
Surija	5.3	178.2	14.5	6,051.36	25	vmu	Y	130	Y	Y	N	2.23	H,S	N	
Susanna	6	93.3	13.2	6,053.37	23	fcOv	Y	71	N	Y	N	3.5	H,S	N	Postdates ARF formation
Taglioni	41.7	122.6	31	6,051.47	12	bst	Y	90	Y	Y	Y	1.59	H,S	N	
Tahia[b]	44.2	73.7	9.1	6,050.70	10	bst	Y	x	N	Y	N	2.55	H	N	
Tekarohi	21.2	76.5	8.9	6,051.69	22	bst	Y	x	N	Y	N	2.86	H,S	N	
Tinyl	9.7	132.1	11.7	6,051.49	24	bst	Y	x	N	Y	N	2.55	H,S	Y	Likely postdates ARF formation, but affected by local reactivation of ARF
Tseraskaya	28.6	79.3	30.1	6,051.64	10	rtT	Y	x	Y	Y	Y	2.86	H,S	N	
Tsiala[b]	2.9	100	16	6,054.83	23	rtO	Y?	x	N	Y	N	3.82	H,S	N	
Ualinka	13.2	168.6	8.1	6,051.97	25	vmu	Y	x	N	Y	N	2.86	H,S	N	
Udyaka	30.8	172.9	12.2	6,051.36	13	vmu	Y	130	N	Y	N	1.59	H,S	N	Postdates ACWR formation
Unay	53.5	172.6	10.8	6,050.83	4	vmu	Y	40	N	Y	N	1.59	H,S	N	
unnamed[b]	5.8	84.3	5.3	6,052.16	22	vmu	Y?	60	N	Y	N	2.55	H,S	N	
unnamed[b]	8	148	7.7	6,051.71	24	st	N	x	N	N	N	3.18	H,S	N	
unnamed[b]	35.8	164.4	5.9	6,051.13	13	vmu	Y?	80	N	Y	N	1.59	H,S	N	
unnamed[b]	6.4	83.4	5.1	6,052.00	22	vmu	Y?	80	N	Y	Y	2.55	H,S	N	
unnamed[b]	55	124.5	4.8	6,051.51	4	fmJ	Y	x	N	Y	N	2.55	H,S	N	
unnamed[b]	40.3	105.9	4.4	6,051.71	11	vmu	Y	x	N	Y	Y	1.59	H	N	
unnamed	38.7	114.7	4.3	6,050.90	11	st	Y	30	N	Y	N	1.59	H	N	
unnamed[b]	7.9	74.2	4.2	6,051.89	22	vmu	Y	x	N	Y	N	2.55	H,S	N	
unnamed[b]	52.1	123.2	4	6,051.61	4	fmJ	Y	80	N	Y	N	2.23	H,S	N	
unnamed	43	150.9	3.9	6,051.05	13	vmu	Y?	40	N	Y	N	2.86	H,S	N	

Table 1
Continued

Name	Latitude (°N)[a]	Longitude (°E)[a]	Diameter (km)[a]	Elevation[a]	Vmap	Units	Ejecta blanket[a]	Impact halo (km)[a]	Central Peak[a]	Rim[a]	Dark Floor[a]	Crater density[a]	Crater database	Deformed[a]	Temporal implications
unnamed[b]	10.4	136.5	3.8	6,051.48	24	vmu	Y	x	N	Y	N	2.23	H,S	N	Postdates formation of ARF
unnamed	42.7	141.7	3.8	6,051.52	12	vmu	Y?	70	N	Y	N	3.5	H,S	N	
unnamed[b]	13.2	112.8	3.7	6,051.24	23	bst	Y?	x	N	Y	N	1.91	H	N	
unnamed[b]	13.33	123.46	1.9		24	btu		x	N	Y	N		S	N	
unnamed[b]	11.9	132.3	3.6	6,051.54	24	bst	Y?	x	N	Y	N	2.86	H,S	N	
unnamed[b]	15.1	116.8	3.6	6,051.63	23	bst	Y	80	N	Y	N	3.5	H,S	N	
unnamedb	43.3	67.7	3.6	6,050.70	10	vmu	Y	x	N	Y	N	1.91	H,S	N	
unnamed	22.6	94.1	3.1	6,051.43	23	bst	Y	x	N	Y	Y	2.23	H,S	N	
unnamed	29.6	135.4	2.7	6,051.14	12	vmu	Y	20	N	Y	N	0.95	H,S	N	
unnamed[b]	8.5	132.4	4.3	6,051.60	24	bst	Y	x	N	Y	N	2.55	H,S	N	Postdates formation of ARF
Valentina	46.4	144.1	24.3	6,051.39	12	vmu	Y	x	Y	Y	Y	4.14	H,S	N	
Vallija	26.3	120	15	6,050.93	11	vmu	Y	200	N	Y	Y	2.86	H,S	N	Postdates formation of ARF and ACWR
Vigee-Lebrun	17.3	141.4	57.6	6,051.06	24	vmu, bst	Y?	x	N	Y	Y	2.55	H,S	N	Postdates formation of NW fractures and ACWR
Wharton	55.6	61.9	50	6,051.76	3	sf	Y	140	N	Y	Y	1.27	H,S	Y	
Wilder	17.4	122.6	35.3	6,052.02	24	rtGe, bst	Y	x	Y	Y	Y	3.18	H,S	N	
Winema	3	168.6	21.1	6,051.58	25	fcRu2	Y	x	N	Y	Y	3.18	H,S	N	Postdates N-trending folds
Yakyt	2.1	170.2	13.8	6,052.19	25	fcRu2	Y	x	Y	Y	Y?	3.5	H,S	Y	Predates final activity along N-trending fractures
Yazruk	21.2	160.2	10	6,051.12	25	fcI	Y	170	N	Y	N	1.27	H,S	N	
Yolanda	7.8	152.7	11.1	6,051.76	25	vmu	Y	40	Y	Y	N	1.91	H,S	N	Postdates ARF formation
Ytunde	49.9	81.1	7.7	6,051.57	10	sf	Y	x	N	Y	N	1.59	H,S	Y?	
Zivile	48.8	113.1	11	6,051.83	11	sf	Y	135	N	Y	N	2.55	H,S	N	Postdates ARF formation
Zulfiya	18.4	101.9	12.3	6,051.63	23	bst, st	Y	x	N	Y	N	2.55	H,S	N	Postdates ARF formation, although ARF may also been locally reactivated
Zumrad	32.1	94.8	12.9	6,051.16	11	bst	Y	60	N	Y	N	1.91	H,S	N	Postdates ARF formation

Note. Dark floor: Materials in the crater floor with the same radar reflectivity than surrounding volcanic materials. Interpreted as possible embayed. Venus crater data bases: S, Schaber et al. (1992); H, Herrick et al. (1997). Crater density values from Herrick et al. (1997) at a crater's location. Value is the density of craters in the neighborhood of the specified crater; that is, the number of craters (including the specified crater) within a 1,000 km radius circle normalized to give the number of craters per 1 × 106 km^2. N, no; U, unknown; Y, yes; ACRW, Artemis concentric wrinkle ridges; ARF, Artemis radial fractures.
[a]Obtained from Herrick et al. (1997). [b]Craters not represented in map because of size and map resolution.

respectively), or a descriptive term such as undivided (btu). These surfaces are termed terrains because it is unclear how many individual units might be represented, but the regions share suites or a suite of tectonic structures that formed prior to the emplacement of adjacent material. Local basal terrain exposures are just that, local, and there is no implication of shared histories between spatially separated basal terrain units across the NMA. However, it is also possible that isolated basal terrain exposures could locally represent temporal equivalent surfaces, or more likely perhaps, represent temporally equivalent unconformity bound packages (i.e., allostratigraphic surfaces/packages).

4.2.1.3. Shield Terrain

Shield terrain consists of thousands of individual shields and coalesced flow materials, referred to as "shield paint" for its apparent low viscosity during emplacement (Hansen, 2005; see also Aubele, 1996). Shield paint could be formed from any combination of lava flows, air-fall deposits, or pyroclastic flows (Crumpler et al., 1997; Guest et al., 1992). Shield terrain contains rocks with an interpreted shared emplacement mechanism (represented by primary structures), which differs from ribbon-tessera terrain whose elements include an interpreted shared deformation history represented by secondary structures.

Within NMA, shield terrain material (unit st) is marked by distributed small (~1–10 km in diameter) shield edifices and their associated deposits. Unit st generally hosts a high density of shields although individual shield is not delineated within NMA due to the map scale. The contact of unit st with adjacent units can locally be sharp but is mostly gradational due to the point source nature of the volcanic activity. Unit st almost certainly represents a time-transgressive unit across the NMA (e.g., Addington, 2001; Stofan et al., 2005), composed of thousands of small edifices that may represent point-source, in situ, partial melting (Hansen, 2005). This unit name is used in a descriptive fashion and does not imply temporal constraints.

We defined a unit transitional between shield and basal terrains, *basal-shield transitional terrain* (unit bst), wherein the discontinuous presence of shields and the low thickness of associated deposits reveal the tectonic structures of the underlying basal terrain. Similarly we locally observe other volcanic features (e.g., intermediate volcanoes and small coronae) partially embayed by shield terrain. Locally stratigraphic relations between such units and shield terrain are difficult to constrain due to the presence of shields in both units and to the point-source character of volcanism; we interpret a diachronic temporal relation between such units.

4.2.2. Material Units

4.2.2.1. Volcanic Material Undivided

Volcanic material undivided (unit vmu) represents a composite unit without stratigraphic significance that combines materials of different origin, and probably different age, that cannot be confidently differentiated with the available data. We use the unit name, volcanic material undivided, because the unit includes many different volcanic styles and radar textures, including corona-, volcano-, and shield-related material of low to intermediate-high backscatter and homogeneous to mottled texture. Volcanic and large tectonomagmatic features are distributed across unit vmu. Large flow units are difficult to delimit, perhaps due to the radar homogenization of the flows with time (Arvidson et al., 1992). Primary structures (e.g., channels, shields, and flow fronts) provide evidence of the multiple genetic processes and distinct source locations for the materials that form the unit. Except for younger materials with clear contact relationships with these volcanic materials, most of the contacts of this unit are delineated as approximate or gradational when these units are in contact with basal-shield transitional and shield terrains; individual shields are also present in this unit.

4.2.2.2. Volcano-Related Flows, Fracture Fed Flows

Several flow units in the NMA are variably associated with different types of volcanic structures (e.g., montes, tholi, paterae, and fields of small volcanoes or colles) and can be differentiated from the undivided material. Each of these material units include the name of their associated volcanic feature (e.g., fmL, Lahar Mons flow material; fthE, Ezili Tholus flow material; fpM, Malintzin Patera; fsA, Aserat Colles shield fields and associated flows). The nature of the contacts varies for the different units; some units display clear flow margins that allow delineation of contacts with sharp transitions; in other cases approximate contacts reflect situations in which the areal limit of the unit is not clear due to the nature and orientation of the radar contact and the interaction with secondary structures. Flow units associated with shield fields (e.g., units fsL and fsJ) display gradational contacts due to the point sourced nature of this type of volcanism. We differentiate these units from the shield terrain due to the larger size of the shields that form the volcanic field, the presence of associated flows and the local temporal relationship with unit vmu and other corona- and volcano-related units (i.e., locally postdate unit vmu). This differentiation between shield terrain and younger shield fields has been noted elsewhere on Venus (Addington, 2001).

4.2.2.3. Corona-Related Material

Many units within the NMA are corona-related deposits. The majority of the corona-related material units are spatially associated with individual coronae as indicated by the material unit name (e.g., fcI, Ituana Corona flows; fcE, Ereshkigal Corona flows), but in some cases where coronae are close or clustered, the unique origin of flows is unclear, and unit names indicate the names of the coronae or the region where these coronae are located (e.g., fcAt, Atalanta Planitia coronae flows). Some coronae have more than one unit delineated when it is possible to differentiate units at the map scale (e.g., Kunhild Corona), but this is rare among coronae in the NMA. This could indicate different stages of corona evolution (e.g., Copp et al., 1998; Smrekar & Stofan, 1999). Nevertheless, absence of subunits does not mean that multistage corona evolution did not occur, but rather that we cannot identify multiple flows with existing data.

Contacts of corona-related material with locally older units bst and st are delineated as gradational given that individual shields are also present in the corona-related flows. The same applies to contacts between corona-related materials and shield fields and associated flow material.

4.2.2.4. Crater Material

The NMA includes two units that represent crater materials. Crater material undivided (unit cu) includes radar-bright material associated with impact crater formation, including crater ejecta and material inside the crater. Some craters present radar-dark interior deposits indicative of embayment by younger flows that cannot be represented at the scale of the map, although these deposits are visible in medium- and high-resolution images. The presence of such materials in individual craters is noted in the associated crater table (Table 1) but not differentiated in the map. This unit is descriptive with no implications for temporal equivalence across the map area. A second unit, crater associated flows undivided (unit cfu), represents impact melt or fluidized ejecta created by meteorite impact associated with the formation of individual impact craters; the melt could be impact related, fluidized ejecta, or formed as a result of tapping pre-existing subsurface magma. Exposures of this unit in most of the cases are small, and as such, not delineated as individual units associated with specific impact craters. Both units are descriptive, with no implications for temporal equivalence across the map area, these units are time-transgressive having formed in association with individual impact craters and not as lithostratigraphic packages.

4.3. Tectonic Structural Suites

Suites of tectonic structures define local or regional patterns that provide clues to operative tectonic or tectonomagmatic processes. We use the terms local and regional tectonic suites to delineate the different scale of tectonic suites. Local structural suites are generally spatially or geometrically associated with individual tectonomagmatic features such as coronae or montes. The timing of local structural suites likely corresponds to the formation, or stages of formation, of the individual features with which they are associated, although the development of these features and the related structural suites can be time-transgressive.

Regional structural suites describe coherent patterns across larger areas and commonly lack spatial or geometric correlation with individual geomorphic or geographic features. Temporal evolution of regional structural suites can be difficult to constrain given that these suites could form time-transgressively and not necessarily formed at the same time across the expansive region where they are developed. Different surface units may be cut by a suite of regional structures, yet there is no guarantee that the entire suite of structures formed in a geological instance (or that there were not episodes of reactivation), frustrating efforts to interpret robust temporal constraints (Hansen, 2000).

4.3.1. Regional Tectonic Suites

NMA's regional tectonic suites are best preserved within planitiae. Although planitiae are commonly considered featureless, NMA planitiae are characterized by numerous suites of distributed deformation features. The most obvious of these regional suites are contractional wrinkle ridges, low topography sinuous structures spaced a few kilometers apart and up to a few hundred kilometers long that record low (<2%) layer contractional strain. We define two groups or patterns of regional wrinkle ridges: (1) a broadly arcuate wrinkle ridge suite that extends from east to west across the NMA, broadly concentric to Artemis Chasma to the south (Hansen & Olive, 2010); (2) a second regional wrinkle ridge suite, orthogonal to the first one, that fans

10.1029/2020EA001171

from NW-trending in western NMA to NE-trending in eastern NMA; this suite is broadly radial to Artemis Chasma to the south, outside NMA. Four suites of distributed lineaments (interpreted broadly herein as fractures) also occur within the planitiae: (1) a fracture suite radial to Artemis Chasma to the south; (2) a suite of NW-tending lineaments that marks the western termination of Ganis Chasma to the east (Senske et al., 1992); (3) a suite of closely-space NE-trending lineaments; and (4) a suite of closely-spaced NW-trending lineaments. The perspective gained through the collaborative mapping of the AMA (Hansen & López, 2020) and the NMA allows us to assign the regional tectonic suites within the NMA to two groups: (a) suites related to the Artemis superstructure (Hansen & Olive, 2010) and (b) other regional suites.

4.3.1.1. Artemis Superstructure-Related Suites

Structural suites related to the Artemis superstructure include extensive areal footprints (Hansen & López, 2018, 2020; Hansen & Olive, 2010): Artemis radial fractures (ARF; 12,000 km diameter) and Artemis concentric wrinkle ridges (ACWR, 13,000 km diameter). The first suite is broadly defined to include fractures, graben, dikes, lineaments, pit chains, and stoping troughs and describes a pattern radial to Artemis Chasma. This suite extends across most of NMA—well-preserved in central NMA and partly present in the west and southeast. The suite is mostly absent in the northeast, as discussed in the geologic history. In Niobe, Sologon, and Llorona Planitiae several small coronae appear geographically related with ARF (e.g., Kubebe Corona in Llorona Planitia; Allatu, Bumiya, and Dhisana Coronae in Sologon-Niobe Planitiae). These features, referred to as circular-lows (Shankar, 2008), typically lack radial fractures.

The ACWR suite, previously described as circum-Aphrodite wrinkle ridges (Billoti & Suppe, 1999), defines a footprint concentric to Artemis Chasma (Hansen & Olive, 2010). Wrinkle ridges are notably absent within ribbon-tessera and basal terrains, even in high-resolution SAR images; although wrinkle ridges locally cut intratessera basin material. Wrinkle ridges occur right up to the contact between ribbon-tessera terrain, basal terrain, and surrounding units, such as bst, st, and vmu. These relations indicate that ribbon-tessera and basal terrain are not rheologically amenable to wrinkle ridge formation (i.e., these units lack a thin deformable layer), whereas the thin basal-shield transitional terrain, shield-terrain, and unit vmu can form wrinkle ridge structures.

The ACWR suite cuts numerous flows associated with individual coronae or montes, providing clear evidence that such flows predated formation of this huge wrinkle-ridge suite. However, some corona-/mons-associated flows do not host wrinkle ridges; these relations could indicate that these flows formed after the Artemis-concentric wrinkle-ridge forming event or that these flows were rheologically not amenable to wrinkle ridge formation, possibly due to flow thickness, internal flow structure, or composition. For example, most flows associated with Uti Hiata Mons (unit fmU1) do not show obvious development of wrinkle ridges; however, wrinkle ridges clearly cut the distal edges of these flows (unit fmU2). Thus, at least distal flows predated ACWR formation. If these flows post-dated formation of the ACWR suite, we might expect numerous examples illustrating the interaction of flows and pre-existing wrinkle ridge topography; however such relationships are not apparent. Some of the flows (e.g., proximal flows) might be too thick to have been affected by wrinkle ridge formation. It is also possible that Uti Hiata Mons formed during a period when some flows formed before and other flows formed after the Artemis-concentric wrinkle ridge suite. The evolution and construction of a large volcano such as Uti Haita Mons and the formation of a regional suite of wrinkle ridges are both likely to be time-transgressive, and plausibly each could last tens to even hundreds of millions of years.

The ARF and ACWR suites together define the Artemis superstructure, interpreted to have formed in association with the Artemis superplume (Hansen & Olive, 2010). The ARF broadly pre-dates formation of the ACWR. At any one location concentric wrinkle ridges and radial fractures are mutually orthogonal. A second large suite of wrinkle ridges in NMA, orthogonal to ACWR, is interpreted to have formed due to inversion of buried ARF structures. Numerous Artemis-radial fractures locally “end” abruptly where they are buried by younger deposits (e.g., volcanic material, undivided; corona-related flows); the fractures end, but there is a transition into straight wrinkle ridges along trend. We interpret this occurrence of fractures and wrinkle ridges as early formed fractures that were buried and subsequently inverted during regional contraction to form topographically positive lineaments (e.g., DeShon et al., 2000). Thus, we interpret the orthogonal pattern of wrinkle ridges in various planitiae to be the results of Artemis-concentric wrinkle ridges and orthogonal inversion structures.

4.3.1.2. Other Regional Structural Suites

We identify two regional fractures suites. These suites principally deform basal materials but also occur locally in thin deposits that postdate basal units.

The NW-trending regional fracture suite extends across most of the NMA cutting units bst, st, and vmu; it is dominantly developed within bst in central and eastern NMA and also occurs in Leda Planitia, northwest NMA. In Akhtamar Planitia (SW NMA), these fractures are locally restricted to basal materials in Lemkechen Dorsa and surrounding basal terrains. The fractures are closely spaced and relatively short, compared to ARF. Where these fractures cut basal materials and local volcanic materials adjacent to ribbon-tessera terrain, they parallel the trend of adjacent ribbon structures (e.g., locations around Gegute Tessera and Uni Dorsa in Niobe Planitia), consistent with structural reactivation of earlier-formed ribbon structure anistotropy.

NE-trending regional fractures mostly occur in Leda Planitia, and in isolated locations cutting units bst and st in Lowana and Llorona Planitiae. Fractures in Leda Planitia are long and locally recognizable as paired lineaments, indicating that these are mostly likely graben; however, lineament orientation with respect to SAR acquisition is not optimal for characterization. Elsewhere these structures can only be resolved as lineaments and display shorter lengths and closer spacing than in Leda Planitia. It is possible that these lineaments represent different genetic suites with similar orientation.

We suggest that the NW- and NE-trending suites predate ARF. Perhaps the most robust evidence for this relative timing emerges from broad geologic relations in which units vmu and st that locally bury the NW- and NE-trending fracture suites are cut by ARF (e.g., 5°N–20°N/135°E–145°E).

4.3.1.3. Fracture Zones

The only fracture zone in the NMA is associated with the northwestern termination of Ganis Chasma, contrary to the AMA where fracture zones define an extensive tectonic domain (Hansen & López, 2020). The part of Ganis Chasma expressed in the NMA lacks the topographic expression and fracture density that characterize the chasma closer to Atla Regio from which it radiates. Within the NMA spaced fractures and graben preserve the identity of host material they cut: ribbon-tessera terrain (Athena and Nemesis Tesserae), basal terrain, and volcanic materials. Locally, fractures covered by thin volcanic materials form inversion wrinkle ridges.

4.3.2. Local Tectonic Suites

Local tectonic structures display linear, radial, or concentric spatial patterns, typically associated with individual deformation belts, coronae, or large volcanic features. We briefly describe areas of concentrated deformation, followed by suites associated with large tectonomagmatic features.

The NMA hosts several deformation belts (also called ridge belts) that mark topographic boundaries between planitiae; parallelism of belt and internal structural trends varies from belt to belt. Collectively the belts might be considered regional given their broad distribution across the NMA, but we consider the belts as local tectonic features herein: NW-tending Lemkechen and Unelanuhi Dorsum in southwest NMA; NE-trending Mardezh-Ava Dorsa in central western NMA; N-trending Poludnista Dorsa in the southeastern most NMA; and the largest belts consisting of NNE-trending Vedma and Oya Dorsum, and Nephele and Frigg Dorsum, in Atalanta and Vellamo Planitiae, respectively.

NW-trending Uni Dorsa and Lumo and Barballe Dorsum differ from the deformation belts described herein. Uni Dorsa (800 km long) consists of ribbon-tessera with folds parallel to the dorsa (and ribbons normal to the dorsa); the tessera inlier is part of a larger quasi-circular ring of ribbon-tessera terrain together with Likho Tesserae, marking the boundary between Niobe Planitia and Vellamo Planitia. NW-trending Lumo and Barballe Dorsum (500 and 1,200 km long, respectively), spaced ~1,000 km apart, comprise unit btu cut by NW-trending regional fractures.

NW-trending Lemkechen and Unelanuhi Dorsum (200 and 2,600 km long, respectively) form outcrops of discontinuous unit btu that predates local volcanic materials in Akhtamar Planitia. The outcrops are characterized by broad anastomosing dorsum-parallel ridges and folds. Wrinkle ridges that cut the young volcanic materials parallel the ridge belts and internal folds but differ in morphology, size, and spacing.

In northern Akhtamar Planitia, NE-trending Mardezh-Ava Dorsa (900 km long) includes NE-trending folds and fractures formed prior to the emplacement of material of the adjacent volcanic plains.

In southeasternmost NMA, and continuing to the AMA, Poludnista Dorsa (1,500 km long) within Rusalka Planitia comprises a N-trending deformation belt that predated regional wrinkle ridges of the Artemis concentric suite (for a detailed structural analysis of Poludnista Dorsa see Young & Hansen, 2005).

Large deformation belts in Vellamo and Atalanta Planitiae describe a fan-shaped pattern with N-trending Nephele Dorsa (1900 km long) to the west and NNE-trending Vedma (3,350 km long) and Oya (480 km long) Dorsum in the east and NNE-trending Frigg Dorsa in between. Nephele Dorsa forms a narrow belt of isolated exposures of btu; Frigg Dorsa is twice as wide but half the length. Vedma and Oya Dorsum, which collectively extend from ~15°N to 55°N, are characterized by btu, cut by belt-parallel folds. Ribbon-tessera terrain occurs locally within Vedma Dorsa, although at a scale below map resolution. NW-trending lineaments within btu parallel local ribbon-tessera fabric trends. AWCR in the surrounding units trend orthogonal to the deformation belt folds. Locally wrinkle ridges parallel the deformation belts and the expected trend of Artemis-radial fractures at such locations. These relations could be interpreted as reorientation of wrinkle ridges around active (at the time) deformation belts or as reactivation of Artemis radial fractures. Both interpretations support a time-transgressive and nonsingular history of wrinkle ridge formation in the NMA.

Local structural suites associated with individual coronae or volcanic features stand out prominently on the geological map. These suites are mostly radial and concentric fractures, with some isolated examples of volcanotectonic structures that show radial wrinkle ridges or concentric ridges. Individual radial or concentric suites formed during the evolution of their host feature; however there is no temporal equivalence inferred for spatially distinct radial or concentric suites.

Tectonomagmatic features that display local radial suites, interpreted as radiating dike swams (e.g., Ernst & Grosfils, 2001; Grosfils & Head, 1994), are grouped in four locations: (1) Akhtamar Planitia; (2) northern Lowana Planitia; (3) Atalanta Planitia; and (4) the equatorial highlands. Some radial fracture suites can extend great distances from their foci and therefore might be useful as local temporal markers for unit delineation (i.e., Cinacoatl Mons in Atalanta Planitia and Kurukulla Mons in Till-Hanun Planitia).

In Akhtamar Planitia radial fracture suites connect large, otherwise isolated, tectonomagmatic centers (Hatshepsut Patera-H'uraru Corona, Uti Hiata Mons, Kaltash Corona, Kunhild Corona, and Ereshkigal Corona), forming an extensive interconnected suite that might appear similar to regional fracture zones. However, contrary to fracture zones in the AMA, these radial fractures do not obscure the identity of host materials. This tectonomagmatic chain extends southward into the AMA, connecting with an unnamed structured centered at 8°S/72°E and terminating in Ix Chel Chasma south of Ova Regio. This corona chain divides Manatum Tessera (western Ovda) from central Ovda Regio. Potential implications of this segmentation of the equatorial highlands remain to be studied.

In northern Lowana Planitia, radial fractures of Kurukulla Mons progressively change orientation to a N-S trend away from the magmatic center, parallel to the local ARF trend.

In Atalanta Planitia radial fractures with a focus of Cinacoatl Mons, extend >1,000 km to the west with a ENE trend, likely the result of the operative regional stress field away from the volcanic source, at the time of fracture formation.

Similar to radial fractures associated with coronae in Akhtamar Planitia, other large local radial fracture suites occur in the equatorial highlands in the area that separates Thetis Regio and Haasttse-baad/Gegute Tesserae. Rosmerta and Blai Coronae display radial fractures that extend hundreds to thousands of kilometers. Blai Corona connects with Ceres Corona to the southeast, part of the Diana-Dali corona-chasma chain in the AMA (Hansen & López, 2020). The relationship of Rosmerta Corona with corona-chasma chains in the AMA is less clear. To the north, in the volcanic plains of Llorona Planitia, radial fractures of Rosmerta and Blai Coronae trend N.

Other local radial fracture suites associated with small features are typically areal restricted to the vicinity of their respective volcanic centers (e.g., Zaltu Mons and Heqet Corona).

Local concentric fractures are associated with many volcanic features (e.g., paterae-caldera and coronae). Most coronae in central NMA are ascribed to the calderic or circular lows subclass of coronae (e.g., DeLaughter & Jurdy, 1999; Shankar, 2008), characterized by concentric fractures similar to that of volcanic caldera and lacking clear radial fracture suites.

Local folds suites that form concentric to some coronae (e.g., Ituana Corona) could be inversion structures (earlier-formed concentric fractures subsequently covered by thin volcanic flows) or gravity related structures (e.g., Sandwell et al., 1997).

A local suite of radial wrinkle ridges is restricted to Fedosova Patera; outward from the volcanic edifice the wrinkle ridges align with the adjacent ACRW. Different formation mechanisms for the formation of radial wrinkle ridges were discussed by Buczkowski (2006) for the case of Irnini Mons.

4.4. Impact Features

NMA hosts 146 impact craters, ranging from 1.9 to 98.1 km diameter. Table 1 lists impact crater location, diameter, elevation, crater density (e.g., Herrick et al., 1997), host material units, and so forth. Most of the craters are included in existing Venus crater data bases (e.g., Herrick et al., 1997; Schaber et al., 1992). Each impact crater displays an interior, rim, and ejecta deposit (unit cu); 40% have parabolic or halo deposits (e.g., Izenberg et al., 1994). Central peaks are rare for craters with diameters <10 km. Impact crater deposits are shown as unit cu, crater material undivided, representing interior and ejecta deposits associated with local bolide impact. Each impact crater formed during a unique spatial and temporally localized event; therefore, composite unit cu is diachronous across the map area. Thus, unit cu is a descriptive unit and does not imply temporal correlation. About 35–40% of the craters display interiors with radar-smooth material.

Interior materials are too small to be represented at map scale, but their presence is indicated in Table 1. These deposits are interpreted as interior deposits that formed after, and unrelated to, initial impact crater formation (Herrick & Rumpf, 2011; Herrick & Sharpton, 2000; Izenberg et al., 1994; Phillips & Izenberg, 1995). Detailed mapping of Venus impact craters using high-resolution digital elevation models indicates that dark-floored craters with diameter >20 km have an average rim-floor depth of 290 m and rim height (measured from rim to the adjacent surroundings) of 240 m, less than bright-floored craters, indicating significant post-crater volcanic modification of radar-dark floored craters (Herrick & Rumpf, 2011; Herrick & Sharpton, 2000). Thus, dark-floored craters likely predate, rather than post-date, the emplacement of at least some of the adjacent units (Hansen et al., 2000, figure 3 therein, for a possible mechanism). This means that the occurrence of an impact crater on a host unit cannot robustly indicate relatively timing of unit and crater emplacement. Geologic mapping using high-resolution DEMs (e.g., Herrick & Rumpf, 2011) has not been employed in NMA construction.

Temporal relations between impact craters and tectonic events can be difficult to robustly constrain. If an impact crater lies between structural elements that comprise the local tectonic suite, such as wrinkle ridges or spaced fractures, the relative timing of crater formation and tectonic activity cannot be determined (Hansen, 2000). Evidence for crater deformation (or lack thereof) is noted in Table 1 in cases where information can be extracted from map relations. At least nine craters show evidence of deformation; however, an apparent lack of deformation is not a robust positive test for impact crater formation after local tectonic activity given the spaced nature of tectonic deformation fabrics and the point location of individual craters. Of the craters that show deformation, six occur on ribbon-tessera and basal terrains, one on shield terrain and two on corona-related units.

Sixty craters locally cover Artemis-related structures. Twenty-two locally cover or follow Artemis radial fractures; 40 locally cover Artemis concentric wrinkle ridges; two craters locally cover both. Although many of these craters have radar-rough (bright) interiors and halo deposits, consistent with relatively young ages (e.g., Izenberg et al., 1994), at least 27 of the craters that locally cover Artemis tectonic suites have interior fill that matches the radar reflectivity of their surroundings. These relations likely indicate a history of early Artemis-structure formation, followed by impact crater formation, following in turn by interior flooding of these individual craters.

Fifteen craters display crater-associated flow material, unit cfu. Ferrier and Cochram craters present flows that are large enough to be mapped as individual units; however, these flows are included in unit cfu for mapping consistency. Ferrier and Himiko craters reside in regions marked by concentric fracture suites on the flanks of coronae. Both impact craters tapped into subsurface magma chambers, presumably associated with their respective coronae. Given the location of these impact craters on the flanks of coronae, and their associated outflow material, it is likely that their radar smooth interiors also relate to their locations relative to host coronae. The rest of the impact craters is not associated with magmatic centers; these features formed by impact on basal terrains and units bst and st. In these cases, the presumed sources of flows are subsurface magma chambers or magma accumulations near the surface but without manifestation in form of concentric fractures or material produced due to the impact process (i.e., melting of the impacted materials).

These data and observations, independently and taken together with the observation that ~40% of the craters within the NMA show interior fill, indicate that a significant number of impact craters within NMA experienced notable geological events (i.e., interior fill emplacement) after crater formation. These results are contrary to initial surveys of the Venus crater population conducted using NASA Magellan data that concluded that only a few percent of Venus craters were deformed or embayed by volcanic material (Collins et al., 1999; Phillips et al., 1992; Schaber et al., 1992; Strom et al., 1994). These new data are consistent with findings of Herrick and Rumpf (2011) and are difficult to accommodate within the context of catastrophic resurfacing models or any resurfacing models that require the vast majority of Venus impact craters to mark the top of the stratigraphic column (e.g., Basilevsky et al., 1997, 1999; Basilevsky & Head, 1998, 2000, 2002a, 2002b, 2006; Ivanov & Head, 2015a, 2015b; Kreslavsky et al., 2015; Reese et al., 2007; Romeo, 2013; Romeo & Turcotte, 2010; Solomatov & Moresi, 1996; Strom et al., 1994; Turcotte, 1993; Turcotte et al., 1999). Thus, crater relations within the NMA cast doubt on the conclusions of these studies. In addition to the data described herein, a growing number of studies similarly indicate that hypotheses of catastrophic resurfacing or hypotheses that call for late formation of most impact craters on Venus are inconsistent with geologic relations and/or modeling (e.g., Bjonnes et al., 2012; Guest & Stofan, 1999; Herrick & Sharpton, 2000, 2002; Hansen & Young, 2007; Hansen & López, 2010; Hansen & Olive, 2010; Herrick & Rumpf, 2011; O'Rourke & Korenaga, 2015) and collectively challenge assumptions that the Venus crater population represents a limited, young, geologic time period.

5. Geologic History

A rich geologic history emerges from the geologic map of the NMA. Given the absence of elements of regional correlation we define local temporal relationships that help to constrain local geologic histories; however, these local histories cannot confidently be extrapolated across NMA or to Venus globally. Tessera terrain and other basal materials formed locally early, followed broadly by the time-transgressive evolution of the Artemis superstructure, coronae, montes, and lowland volcanic deposits.

Basal ribbon-tessera terrain units formed early across NMA and in a time-transgressive manner. That is, not all ribbon-tessera formed in one event, although these distinctive terrains likely formed within a geological era marked by specific geologic conditions, most notably an era marked by thin global lithosphere (Bindschadler, 1995; Hansen, 2006; Hansen et al., 2000; Phillips & Hansen, 1994).

We distinguish three different groups of ribbon-tessera terrain: (a) within the equatorial crustal plateaus including west and central Ovda Regio and Thetis Regio, (b) within Tellus Regio, and (c) as inliers distributed across the NMA. All three groups of ribbon-tessera terrain present similar tectonic fabrics with local variations in trend and degree of embayment.

Ribbon-tessera tectonic fabric evolved through progressive deformation of a strong thin layer above an extremely low-viscosity layer over a strong substrate (Hansen, 2006), indicating a high heat flow across the areal extent of individual crustal plateaus (Ruiz, 2007), which are characterized by ribbon-tessera terrain. Tectonic fabric evolution was accompanied by formation of local intratessera volcanic basins filled with low-viscosity volcanic materials (Banks & Hansen, 2000; Bindschadler et al., 1992; Gilmore et al., 1998; Hansen, 2006; Hansen et al., 2000; Hansen & Willis, 1996, 1998). Evidence for this style of volcanic activity is preserved in Ovda, Thetis, and Tellus regiones due to high topography (e.g., Banks & Hansen, 2000; Gilmore & Head, 2018). However, clear differentiation between intratessera basin material and significantly younger volcanic material is difficult in tessera inliers due subdued topography (e.g., Haasttse-baad Tessera).

Tectonic patterns in the ribbon-tessera inliers (e.g., Gegute and Haasttse-baad Tesserae in Llorona Planitia, Shimti, Kutue and Ananke Tesserae crossing through Lowana, Niobe and Tilli-Hanun Planitiae; and Nemesis and Athena Tesserae in Atalanta Planitia) show coherent patterns across regions similar in size to that of crustal plateaus (Hansen & López, 2010). Such regionally coherent patterns across such expansive regions is consistent with the idea that ribbon-tessera inliers represent ancient packages similar to those

10.1029/2020EA001171

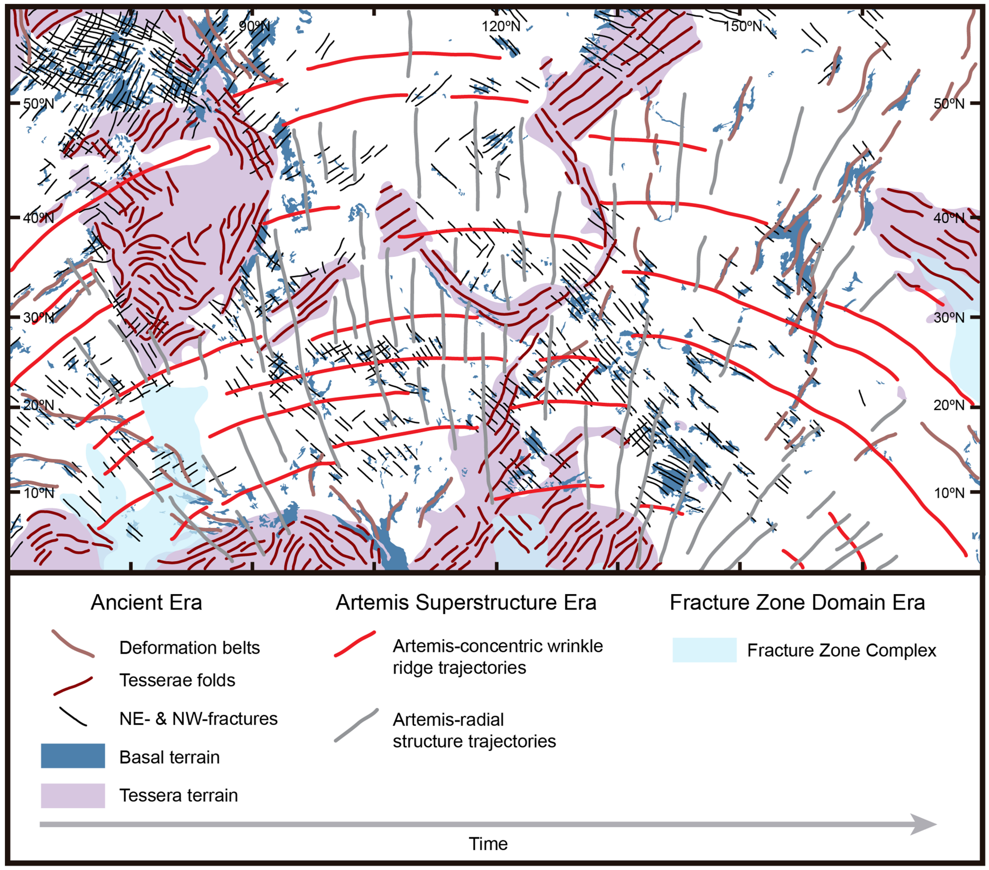

Figure 2. Mercator projection summary of the tectonic regimes within the NMA.

preserved within, and characteristic of, crustal plateaus (Bindschadler, 1995; Hansen & López, 2010; Ivanov & Head, 1996; Phillips & Hansen, 1998).

Assemblages of basal terrain are exposed locally (e.g., unit btL), commonly in contact with ribbon-tessera terrain, and as isolated outcrops or kipukas. Origin of these basal terrains is not clear nor is it required that all basal terrain formed in the same fashion. Basal terrains could have formed before, during, or after the era during which ribbon-tessera terrain formed and could mark areas between regions of ribbon-tessera terrain. Exposures of basal terrain are cut by different tectonic structures. In some locations, these tectonic structures can be resolved only as close-spaced lineaments, but in most cases the tectonic structures appear to be composed of closely spaced fractures. In eastern NMA (e.g., Vedma Dorsa) NNE-trending outcrops of basal terrain are deformed by folds and broad ridges.

In central and western NMA regional NW-trending fractures cut basal terrain, with fractures parallel to adjacent tessera fabric trends; units bst, st, and vmu postdate basal terrain. NW-trending fractures within younger volcanic units are due to incomplete burial, or structural reactivation, or both.

In northwest NMA NE-trending fractures cut basal terrain with fracture trends parallel to adjacent tessera fabric trend; NE-trending fractures both cut and are covered by unit bst. Other local units (e.g., units st and fpHC) display NE-trending wrinkle ridges, parallel to, and in continuation of, fractures of the basal terrain; we interpret these wrinkle ridges as inversion structures of buried fractures (e.g., DeShon et al., 2000). All these previous materials and events would belong to the ancient era.

Various volcanic units, emplaced after tessera and basal terrain deformation, form the NMA volcanic plains. It is difficult to establish a singular chronology across the map area. Although the large tectonic suites of the Artemis superstructure (ARF and ACWR) constrain *relative* temporal relations, evolution of the Artemis superstructure is not temporally constrained. Absolute timing and duration of the Artemis superstructure-related suites cannot be constrained given current data. We follow the suggestion of Hansen and Olive (2010) that the evolution was time-transgressive based on cross-cutting relations. Employing the Artemis superstructure-related suites as unique temporal timelines requires additional data that robustly constrains short-temporal duration of their formation and evolution. No such data are currently available for Venus.

In the lowlands due north of Aphrodite Terra—the volcanic plains, composed mostly of units bst and st, also lack robust temporal relations. Unit st in composed exclusively by small shields, but local exposures of unit bst also present embayed intermediate volcanoes (e.g., López, 2011) and small coronae without evident associated flows (i.e., circular lows).

In general, ARF and ACWR cut units bst and st, although locally individual shields could postdate these tectonics structures. One possible mode of the formation of unit st (or bst) is heating from below, driving in situ partial melting of the overlying crust and subsequent emergence of point-source shield formation. There is a possible spatial association, consistent with (but not requiring) a genetic association, between ribbon-tessera terrain and shield terrain. In western and central NMA, spatial association between units bst and st and ribbon-tessera terrain appears obvious, with large expanses of units bst and st located in and around large ribbon-tessera terrain blocks and inliers. In contrast, units bst and st are rare in Rusalka, Vellamo, and Atalanta Planitiae, all regions that generally lack ribbon-tessera terrain.

Large corona-related flow units that locally postdate units bst and st occupy a large region adjacent to Aphrodite Terra. These units (fcK, fcRo, and fcOv) consist of low viscosity flows that extend great distances and postdate tessera, bst, and st. Unit fcOv is a huge composite unit composed of flows from several coronae and volcanic structures; this unit cannot be used as a detailed a temporal marker. Some of the material is easily traced to specific coronae, such as Kaltash (unit fcK), Rosmerta (fcRo), and Blai (fcB) Coronae. These coronae, which formed on ribbon-tessera terrain, are characterized by large local radial fracture suites and topographically low corona annulus.

In this area it is also difficult to constrain temporal relations between coronae-related fractures and ARF structures. Flows of unit fcOv both cover and are deformed by ARF and ACWR; however, the composite nature of unit fcOv precludes the establishment of reliable temporal relations. Kaltash and Rosmerta Coronae also display well-developed radial fracture suites, which further frustrate efforts to robustly constrain temporal relations with the Artemis-superstructure related suites. Given that ARF do not clearly transect these coronae, we expect that the coronae broadly postdate the formation of ARF or rather that the evolution of these coronae outlasted formation of ARF. However, ACWR cut distal flows sourced from Rosmerta Corona (e.g., unit fcRo). Thus it is possible that the Artemis superstructure began to form prior to the formation of Rosmerta, and formation of Rosmerta temporally overlapped with, and outlasted, that of the Artemis-superstructure.

In Akhtamar Planitia a cluster of tectonovolcanic structures postdate emplacement of local lowland materials. Temporal relations with regard to ARF and ACWR are difficult to constrain given that the local tectonic structures mimic the trends of these regional structures. The cluster formed by Ereshkigal and Kunhild Coronae and their associated materials (units fcE, fcKu1, and fcKu2) has been interpreted as result of the formation of a now-extinct hot-spot (Herrick & MacGovern, 2000). Coronae-related materials are locally covered by younger volcanic flows associated with Ezili Tholus (unit fthE), a flat-topped volcano located northeast of the center of proposed extinct hot-spot (Ezili Tholus could be interpreted as part of late hot-spot evolution). Other large volcanic structures postdate the ARF and ACWR suites in Akhtamar Planitia. Uti Hiata Mons is a complex magmatic system with associated flow units (units fmU1 and fmU2) that locally postdate units bst, st, and vmu and other previous volcanic structures (embayed intermediate volcanoes; see figures 4a and 4f in López, 2011). Hatshepsut Patera (northern Akhtamar Planitia) represents a complex magmatic system composed of concentric fractures that define a caldera surrounded by flow material (unit fpH) and late steep-sided domes.

Collectively Kurukulla Mons, Hiei Chu Patera, Amra Tholus, and several other unnamed volcanic structures comprise a large volcanic cluster located between northern Lowana Planitia and Tilli-hanun Planitia. Contact relations between materials associated with Kurukulla Mons and Hiei Chu Patera (units fmK and fpHC) are difficult to constrain due to the absence of clear radar contacts and the presence of shields in both units; contacts are mapped as approximate. Flows from Amra Tholus and an unnamed volcanic edifice postdate radial fractures of Kurukulla Mons; however, it is not clear if these flows postdate all the activity in Kurukulla Mons or simply the formation of radial fractures. Temporal relations of all these units with respect to ARF and ACWR suites are difficult to determine given that radial fractures of Kurukulla Mons parallel ARF. ACWR cut some parts of units fmK, fpHC, and fpu1; however local wrinkle ridges suites, interpreted as inversion structures, also deform these materials.

In Lowana Planitia volcanic units associated with shield clusters or volcanic fields (units fsSh and fsLw) postdate units bst, st, and vmu. The point-sourced nature of shields and the presence of shields in each unit renders contact delineation difficult; contacts are mapped as gradational.

Central NMA is dominated by units bst and st, which predate ARF and ACWR, and corona- and volcano-related units (fcA, fmUa, and fpJ); the latter units locally bury ARF but are cut by ACWR. In Niobe Planitia we interpret N-trending wrinkle ridges in unit vmu as having formed by structural inversion of ARF structures, with unit vmu locally postdating units bst and st, with Maa-Ema Corona serving as a possible source for unit vmu.

In eastern NMA ribbon-tessera and basal terrain predate emplacement of composite units bst, st, and vmu, and local corona- and volcano-related units (units fcI, fcV, and unit fsL). In Rusalka Planitia corona-related flows locally postdate unit vmu (unit fu of Young & Hansen, 2003). These corona-related materials (units fcRu1 and FcRu2) are in turn locally postdated by small volcano related flows (units fmI, fmLa, and fmM) and volcanic materials associated with shield fields (units fsA, fsR, and fsZy). The areal extent of unit vmu in the eastern NMA is more extensive than elsewhere; however, vmu is a composite unit with potentially many different sources. Unit vmu hosts numerous circular topographic rims that could represent buried coronae and that indeed could be source of at least part of this composite unit in this region. Eastern NMA also hosts a large number of volcanic channels or canali. Baltis Vallis, Venus' longest volcanic channel, runs through most of this part of the map area in unit vmu. Within Rusalka Planitia areally localized volcano-related units (fmZ) and materials related to shields fields (fsRk) postdate unit vmu. These shield-related volcanic materials are locally cut by Ganis Chasma fractures. Ganis Chasma is considered a young feature in the geologic evolution of Venus (Basilevsky, 1998). Both the fracture density and topographic signature of the terminous of Ganis Chasma in the NMA are more muted than in Atla Regio, where recent volcanic activity has been proposed (Shalygin et al., 2015).

In Atalanta Planitia a large corona-related composite unit formed by flows from different volcano-tectonic structures (Holde and Mari Coronae, and Cinacoatl Mons) (unit fcAt) occupies much of northeastern NMA. This unit locally postdates basal materials and unit vmu; distal flows of unit fcAt postdate Baltis Vallis in Atalanta Planitia. These corona-related materials are locally covered by small shields and associated flows from Jurate Colles (unit fsJ) that also postdate unit vmu and tessera terrain of Ananke Tessera. Other local volcanic units sourced from fractures and volcanic centers postdate unit vmu in Atalanta Planitia (units fpF, fpu2, and ffr).

In western NMA the ACWR suite is well-developed. NW-trending fractures could represent ARF, or fractures related to coronae and/or montes, or both; the trends fit both interpretations. Vellamo, Atalanta, and Rusalka Planitiae display two suites of mutually orthogonal wrinkle ridges—ACWR and parallel to ARF. It is likely that the latter suite represents buried ARF (by unit vmu) reactivated as inversion structures (e.g., DeShon et al., 2000).

In general, the geologic history of the NMA is complex and diverse, with multitude of volcanic units that postdate basement materials. Most of these volcanic materials form composite units, and we stress the importance that point-sourced volcanic activity played in the geologic evolution of the NMA (units bst and st), as first noted by Aubele (1996). There also appears to be a broad spatial association of these units to ribbon-tessera inliers. Numerous coronae and large volcanoes form local clusters that postdate basement materials and basal plain materials (units bst and st). The main regional tectonic suites are related to the formation and evolution of the Artemis superstructure and can be used as a local relative temporal marker; however, one must be cognizant that the duration of Artemis superstructure evolution is unknown. Other regional and local tectonic suites deform the NMA materials and interact with volcanic flows depicting a rich and complex geologic history that can only be constrained locally in absence of reliable temporal markers.

10.1029/2020EA001171

Geologic relations preserved within the NMA do not support catastrophic resurfacing models but instead are consistent with complex geologic evolution of the Venusian lowlands.

6. Conclusions

The geologic mapping of the NMA provide first-order observations and/or geologic implications enumerated below.

1. Geologic mapping of the NMA supports observations made in the AMA that show broad geologic domains and broad cross-cutting temporal relationships in this part of the planet. Patterns are mostly defined by the mapping of structural elements that show coherent patterns across both map areas (Hansen & López, 2018). The three tectonic domains defined in both map areas include, from oldest to youngest (Figure 2): (1) an Ancient era represented by ribbon-tessera terrain (including intra-tessera basin material) in both crustal plateaus and lowland inliers, and locally developed basal terrain; (2) structures associated with the development of the Artemis superstructure, including Artemis-radial fractures and -concentric wrinkle ridge suites; and (3) a younger era characterized by the development of fracture zone terrain, including chains of coronae and chasmata.
2. The Ancient era is well represented by different lithodemic units distributed across the NMA (Figure 2). Ribbon-tessera terrain is found within the equatorial crustal plateaus (west and central Ovda Regio and Thetis Regio), Tellus Regio, and as inliers of different size scattered across the map area. Ribbon-tessera terrain units formed early across NMA and in a time-transgressive manner in an era marked by thin global lithosphere. Other assemblages of basal terrain are locally exposed basal terrains that could have formed before, during, or after the era during which ribbon-tessera terrain formed and could mark areas between regions of ribbon-tessera terrain.
3. Shield terrain, a unique style of volcanic unit first recognized and described by Aubele (1996) in Niobe Planitia and later characterized in detail by Hansen (2005), occurs across much of NMA. Shield terrain postdates ribbon-tessera terrain inliers and basal terrains in the lowland; however its evolution requires further study. This lithodemic unit likely formed broadly time-transgressive; it is not clear if formation of shield terrain started in the ancient era or later in the history of the volcanic plains, or both. Evidence for formation of shield terrain late within the ancient era, but perhaps relatively early within the Artemis superplume era includes: The occurrence of transitional materials between shield terrain and the basal units and that shield terrain both cuts and is cut by Artemis Chasma-radial fractures; and yet Artemis Chasma-concentric wrinkle ridges (which postdate the ARF suite) generally cut shield terrain deposits. These relations lead most directly to temporal constraints in which shield terrain within the NMA formed prior to and/or early during the evolution of the Artemis superstructure (i.e., overlapping in time with the formation of the ARF suite) and was broadly emplaced prior to development of the extensive Artemis Chasma-concentric wrinkle-ridge suite—which represents late-stage evolution of this huge structure (Hansen & Olive, 2010). One would/could expect that the geologic transition between the ancient era and the Artemis superstructure era might be time-transgressive, rather than geologically catastrophic.
4. Artemis-radial fractures and Artemis-concentric wrinkle ridges defined regional patterns relative to Artemis Chasma (12,000 and ~13,000 km diameters, respectively) irrespective of the material units they deform (Figure 2), consistent with geologic relations documented within the AMA. Artemis radial fractures are more difficult to define in the NMA than in the AMA due to the distance to Artemis Chasma; the location of the Aphrodite Terra crustal plateaus between Artemis Chasma and the NMA lowlands; and the occurrence of, and interaction with, other local tectonic suites. However, regional-scale map relations documented in both the AMA and the NMA together illustrate a clear pattern. Somewhat in contrast, the regional pattern of the Artemis-concentric wrinkle ridge suite is quite clearly defined within the NMA, particularly in southern and central NMA; equally important, this extensive wrinkle ridge suite is difficult to define in the north part of the NMA, marking the boundary or spatial termination of this extensive suite. By comparison, the boundaries of this suite lie outside the spatial limit of the AMA and extend to the south of that map area (Figure 1b).
5. Undivided volcanic materials, and also materials and local tectonic suites associated with individual tectonovolcanic structures postdate materials and structures of the ancient era. Much of this material likely formed during the era related to the evolution of the Artemis superstructure or during the transition of

this era to the youngest fracture zone era. It is difficult to establish a singular chronology across the map area. Although the large tectonic suites of the Artemis superstructure constrain some temporal relations, evolution of the Artemis superstructure is not temporally constrained and likely time transgressive. Therefore, these suites cannot impose robust temporal constraints. Some tectonovolcanic structures seem to postdate, or at least have outlasted, formation of the Artemis superstructure given that associated flows are not apparently deformed by the Artemis-concentric wrinkle-ridge suite. However, such flows could also predate wrinkle-ridge formation, given that individual flows, or parts of flows, could be rheologically unfavorable to the formation of wrinkle ridges. Geologic relations documented within NMA are consistent with a time-transgressive transition from the Artemis superstructure era to the fracture zone era.

6. Evidence for the fracture zone era is little represented in the NMA compared to the AMA. In the NMA we observe the termination of fracture zones (e.g., Ganis Chasma) where fracture density is lower than in the fracture zones observed in the AMA and where precursor materials can be observed. Coronae within NMA, particularly those near the southern boundary with AMA (e.g., Blai, Rosmetra, and Kaltash Coronae) could represent distal limits of the fracture zone domain, which includes coronae and chasmata. Further study, including more detailed geologic mapping, may shed light on these relationships.
7. Impact craters clearly formed time-transgressively across the NMA relative to each of the three major geologic eras noted above; nearly half of the craters within the NMA show interior fill, indicating that a significant number of impact craters within NMA experienced notable geological events (i.e., interior fill emplacement) after impact crater formation. Thus, there is no geologic evidence within the NMA that impact craters lie at the highest level of NMA stratigraphy or that impact craters mark the youngest "event" across the NMA. Furthermore, geologic relations do not require and in fact provide strong evidence against global-scale catastrophic resurfacing of Venus.
8. NMA materials and structures depict a rich and complex geologic history that can only be constrained locally in the absence of reliable temporal markers. Geologic relations preserved within the NMA are consistent with a complex geologic evolution of the Venusian lowlands.

In summary, the picture that emerges is the regional coherence of preserved geologic patterns in this part of the planet (both AMA and NMA) that record three relatively distinct geologic eras with the first two particularly well recorded within the NMA (Hansen & López, 2018). The three eras are relatively distinct in terms of the geologic elements that define them. However, the temporal transition from one era to the next does not appear to be sharply defined and as such may represent global-scale geodynamic transitions indicative perhaps of transitional geodynamic processes. Future geologic mapping of the rest of Venus, at a similar scale to that presented herein, will add important spatial and temporal information regarding the evolution of these three geologic eras and could also lead to the identification of other geologic eras within the evolution of Earth's sister planet Venus.

Data Availability Statement

Base maps used for geologic mapping are available free in Zenodo (López & Hansen, 2020, http://doi.org/10.5281/zenodo.3712688). NASA Magellan data are also available via USGS Map a Planet website (https://astrogeology.usgs.gov/tools/map-a-planet-2).

Conflict of Interest

The authors have no financial conflicts of interests or other conflicts of interest with regard to this work.

Acknowledgments
Geologic mapping was supported by National Aeronautics and Space Administration (award NNX12AQ71G). V. L. H. gratefully acknowledges support from the McKnight Foundation and the University of Minnesota. The authors thank D. A. Williams and R. E. Ernst for their thoughtful reviews and editor Kirsty Tiampo for her comments and guidance.

References

Addington, E. A. (2001). A stratigraphic study of small volcano clusters on Venus. *Icarus*, *149*(1), 16–36. https://doi.org/10.1006/icar.2000.6529
Arvidson, R. E., Baker, V. R., Elachi, C., Saunders, R. S., & Wood, J. A. (1991). Magellan: Initial analysis of Venus surface modification. *Science*, *252*(5003), 270–275. https://doi.org/10.1126/science.252.5003.270
Arvidson, R. E., Greeley, R., Malin, M. C., Saunders, R. S., Izenberg, N., Plaut, J. J., et al. (1992). Surface modification of Venus as inferred from Magellan observation of plains. *Journal of Geophysical Research*, *97*(E8), 13,303–13,318. https://doi.org/10.1029/92JE01384
Aubele, J. (1996). Akkruva small shield plains; definition of a significant regional plains unit on Venus. *Abstracts of the Lunar and Planetary Science Conference XXVII* (pp. 49–50). Houston, Texas.

Baker, V. R., Komatsu, G., Gulick, V. C., & Parker, T. J. (1997). Channels and valleys. In S. W. Bouger, D. M. Hunten, & R. J. Phillips (Eds.), (pp. 757–798). *Venus II: Geology, Geophysics, Atmosphere, and Solar Wind Environment*, Tucson: University of Arizona Press.

Baker, V. R., Komatsu, G., Parker, T. J., Gulick, V. C., Kargel, J. S., & Lewis, J. S. (1992). Channels and valleys on Venus—Preliminary analysis of Magellan data. *Journal of Geophysical Research*, *97*, 13,395–13,420. https://doi.org/10.1029/92JE00927

Banerdt, W. B., McGill, G. E., & Zuber, M. T. (1997). Plains tectonics on Venus. In S. W. Bouger, D. M. Hunten, & R. J. Phillips (Eds.), (pp. 901–930). *Venus II: Geology, Geophysics, Atmosphere, and Solar Wind Environment*,Tucson: University of Arizona Press.

Banks, B. K., & Hansen, V. L. (2000). Relative timing of crustal plateau magmatism and tectonism at Tellus Regio, Venus. *Journal of Geophysical Research*, *105*(E7), 17,655–17,667. https://doi.org/10.1029/1999JE001205

Basilevsky, A. T. (1998). Age of rifting and associated volcanism in Atla Regio, Venus. *Geophysical Research Letters*, *20*, 883–886.

Basilevsky, A. T., & Head, J. W. (1996). Evidence for rapid and widespread emplacement of volcanic lains on Venus: Stratigraphic studies in the Baltis Vallis region. *Geophysical Research Letters*, *23*(12), 1497–1500. https://doi.org/10.1029/96GL00975

Basilevsky, A. T., & Head, J. W. (1998). The geologic history of Venus: A stratigraphic view. *Journal of Geophysical Research*, *103*(E4), 8531–8544. https://doi.org/10.1029/98JE00487

Basilevsky, A. T., & Head, J. W. (2000). Geologic units on Venus: Evidence for their global correlation. *Planetary and Space Science*, *48*(1), 75–111. https://doi.org/10.1016/S0032-0633(99)00083-5

Basilevsky, A. T., & Head, J. W. (2002a). On the rates and styles of late volcanism and rifting on Venus. *Journal of Geophysical Research*, *107*(E6), 5041. https://doi.org/10.1029/2000JE001471

Basilevsky, A. T., & Head, J. W. (2002b). Venus: Timing and rates of geologic activity. *Geology*, *30*(11), 1015–1018. https://doi.org/10.1130/0091-7613(2002)030<1015:VTAROG>2.0.CO;2

Basilevsky, A. T., & Head, J. W. (2006). Impact craters on regional plains on Venus: Age relations with wrinkle ridges and implications for the geological evolution of Venus. *Journal of Geophysical Research*, *111*, E03006. https://doi.org/10.1029/2005JE002473

Basilevsky, A. T., Head, J. W., Ivanov, M. A., & Kryuchkov, V. P. (1999). Impact craters on geologic units of northern Venus: Implications for the duration of the transition from tessera to regional plains. *Geophysical Research Letters*, *26*(16), 2593–2596. https://doi.org/10.1029/1999GL008329

Basilevsky, A. T., Head, J. W., Schaber, G. G., & Strom, R. G. (1997). The resurfacing history of Venus. In S. W. Bouger, D. M. Hunten, & R. J. Phillips (Eds.), (pp. 1047–1086). *Venus II: Geology, Geophysics, Atmosphere, and Solar Wind Environment*, Tucson: University of Arizona Press.

Billoti, F., & Suppe, J. (1999). The global distribution of wrinkle ridges on Venus. *Icarus*, *139*(1), 137–157. https://doi.org/10.1006/icar.1999.6092

Bindschadler, D. L. (1995). Magellan: A new view of Venus' geology and geophysics. *Reviews of Geophysics*, *33*, 459–467. https://doi.org/10.1029/95RG00281

Bindschadler, D. L., deCharon, A., Beratan, K. K., & Head, J. W. (1992). Magellan observations of Alpha Regio—Implications for formation of complex ridged terrains on Venus. *Journal of Geophysical Research*, *97*(E8), 13,563–13,577. https://doi.org/10.1029/92JE01332

Bjonnes, E. E., Hansen, V. L., James, B., & Swenson, J. B. (2012). Equilibrium resurfacing of Venus: Results from new Monte Carlo modeling and implications for Venus surface histories. *Icarus*, *217*(2), 451–461. https://doi.org/10.1016/j.icarus.2011.03.033

Bleamaster, L. F., III, & Hansen, V. L. (2005). Geologic map of the Ovda Regio quadrangle (V-35), Venus. *U.S. Geological Survey Scientific Investigations Map* I-2802, 1:5,000,000, http://pubs.usgs.gov/imap/i2808/

Brown, C. D., & Grimm, R. E. (1999). Recent tectonic and lithospheric thermal evolution of Venus. *Icarus*, *139*(1), 40–48. https://doi.org/10.1006/icar.1999.6083

Buczkowski, D. L. (2006). Kinematic analysis of radial structures around Irnini Mons, Venus. *Journal of Structural Geology*, *28*(12), 2156–2168. https://doi.org/10.1016/j.jsg.2006.04.005

Bussey, D. B. J., Sorenson, S. A., & Guest, J. E. (1995). Factors influencing the capability of lava to erode its substrate: Application to Venus. *Journal of Geophysical Research*, *100*(E8), 16,941–16,948. https://doi.org/10.1029/95JE00894

Butler, B. C. M., & Bell, J. D. (1988). Interpretation of geological maps, 232 pp., Longman Science & Technical, Essex. England: Longman Scientific & Technical; New York.

Campbell, B. A. (1999). Surface formation rates and impact crater densities on Venus. *Journal of Geophysical Research*, *104*(E9), 21,951–21,955. https://doi.org/10.1029/1998JE000607

Campbell, B. A., Campbell, D. B., Morgan, G. A., Carter, L. M., Nolan, M. C., & Chandler, J. F. (2015). Evidence of crater ejecta on Venus tessera terrain from Earth-based radar images. *Icarus*, *250*, 123–130. https://doi.org/10.1016/j.icarus.2014.11.025

Campbell, D. B., Stacy, N. J. S., Newman, W. I., Arvidson, R. E., Jones, E. M., Musser, G. S., et al. (1992). Magellan observations of extended impact crater related features on the surface of Venus. *Journal of Geophysical Research*, *97*(E10), 16,249–16,277. https://doi.org/10.1029/92JE01634

Collins, G. C., Head, J. W., Basilevsky, A. T., & Ivanov, M. A. (1999). Evidence for rapid regional plains emplacement on Venus from the population of volcanically embayed impact craters. *Journal of Geophysical Research*, *104*(E10), 24,121–24,139. https://doi.org/10.1029/1999JE001041

Compton, R. R. (1985). *Geology in the field* (p. 398). New York, NY: John Wiley & Sons.

Copp, D. L., Guest, J. E., & Stofan, E. R. (1998). New insights into coronae evolution: Mapping on Venus. *Journal of Geophysical Research*, *103*(E8), 19,401–19,417. https://doi.org/10.1029/97JE03182

Crumpler, L. S., Aubele, J. C., Senske, D. A., Keddie, S. T., Magee, K. P., & Head, J. W. (1997). Volcanoes and centers of volcanism on Venus. In S. W. Bouger, D. M. Hunten, & R. J. Phillips (Eds.), *Venus II—Geology, geophysics, atmosphere, and solar wind environment* (pp. 697–756). Tucson: University of Arizona Press.

Cushing, G. E., Okubo, C. H., & Titus, T. N. (2015). Atypical pit craters on Mars. New insights from THEMIS, CTX, and HiRISE observations. *Journal of Geophysical Research: Planets*, *120*, 1023–1043. https://doi.org/10.1002/2014JE004735

DeLaughter, J. E., & Jurdy, D. M. (1999). Corona classification by evolutionary age. *Icarus*, *139*(1), 81–92. https://doi.org/10.1006/icar.1999.6087

DeShon, H. R., Young, D. A., & Hansen, V. L. (2000). Geologic evolution of southern Rusalka Planitia, Venus. *Journal of Geophysical Research*, *105*(E3), 6983–6995. https://doi.org/10.1029/1999JE001155

Easton, R. M., Edwards, L. E., Orndorff, R. C., Duguet, M., & Ferrusquia-Villafranca, I. (2016). North American commission on stratigraphic nomenclature North American Commission On Stratigraphic Nomenclature Report 12—Revision of article 37, Lithodemic Units, of the North American Stratigraphic Code. *Stratigraphy*, *13*(3), 220–222.

Easton, R. M., Jones, J. O., Lenz, A. C., Ferrusqua-Villafranca, I., Mancini, E. A., Wardlaw, B. R., et al. (2005). North American commission on stratigraphic nomenclature. *AAPG Bulletin*, *89*, 1459–1464. https://doi.org/10.1306/05230505015

Ernst, R. E., Desnoyers, E. W., Head, J. W., & Grosfils, E. B. (2003). Graben-fissure systems in Guinevere Planitia and Beta Regio (264°–312°E, 24°–60°N), Venus, and implications for regional stratigraphy and mantle plumes. *Icarus*, *164*(2), 282–316. https://doi.org/10.1016/S0019-1035(03)00126-X

Ernst, R. E., Grosfils, E. B., & Mège, D. (2001). Giant dike swarms: Earth Venus and Mars. *Annual Review of Earth and Planetary Sciences*, *29*(1), 489–534. https://doi.org/10.1146/annurev.earth.29.1.489

Ferrill, D. A., Wyrick, D. Y., Morris, A. P., Sims, D. W., & Franklin, N. M. (2004). Dilational fault slip and pit chain formation on Mars. *GSA Today*, *14*, 1–9. https://doi.org/10.1130/1052-5173(2004)014<4:dfsapc>2.0.co;2

Ford, J. P., Plaut, J. J., Weitz, C. M., Farr, T. G., Senske, D. A., Stofan, E. R., et al. (1993). Guide to Magellan image interpretation. *National Aeronautics and Space Administration Jet Propulsion Laboratory Publication*, 93(24), 148. Pasadena, CA.

Ghent, R. R., & Hansen, V. L. (1999). Structural and kinematic analysis of eastern Ovda Regio, Venus: Implications for crustal plateau formation. *Icarus*, *139*(1), 116–136. https://doi.org/10.1006/icar.1999.6085

Gilbert, G. K. (1886). Inculcation of the scientific method. *American Journal Science*, *31*, 284–299. https://doi.org/10.2475/ajs.s3-31.184.284

Gilmore, M. S., Collins, G. C., Ivanov, M. A., Marinangeli, L., & Head, J. W. (1998). Style and sequence of extensional structures in tessera terrain, Venus. *Journal of Geophysical Research*, *103*(E7), 16,813–16,840. https://doi.org/10.1029/98JE01322

Gilmore, M. S., & Head, J. W. (2018). Morphology and deformational history of Tellus Regio, Venus: Evidence for assembly and collision. *Planetary and Space Science*, *154*, 5–20. https://doi.org/10.1016/j.pss.2018.02.001

Gregg, T. K. P., & Greely, R. (1993). Formation of Venusian canali: Considerations of lava types and their thermal behaviors. *Journal of Geophysical Research*, *98*(E6), 10,873–10,882. https://doi.org/10.1029/93JE00692

Grindrod, P. M., & Guest, J. E. (2006). 1:1.5,000,000 geological map of the Aglaonice region on Venus. *Journal of Maps*, *2*, 103–117. https://doi.org/10.4113/jom.2006.57

Grosfils, E. B., & Head, J. W. (1994). The global distribution of giant radiating dike swarms on Venus: Implications for the global stress state. *Geophysical Research Letters*, *21*(8), 701–704. https://doi.org/10.1029/94GL00592

Guest, J. E., Bulmer, M. H., Aubele, J. C., Beratan, K., Greely, R., Head, J. W., et al. (1992). Small volcanic edifices and volcanism in the plains on Venus. *Journal of Geophysical Research*, *97*(E10), 15,949–15,966. https://doi.org/10.1029/92JE01438

Guest, J. E., & Stofan, E. R. (1999). A new view of the stratigraphic history of Venus. *Icarus*, *139*(1), 55–66. https://doi.org/10.1006/icar.1999.6091

Hanmer, S. (2020). Tessera terrain ribbon fabrics on Venus reviewed: Could they be dyke swarms? *Earth-Science Reviews*, *201*, 10,3077. https://doi.org/10.1016/j.earscirev.2019.103077

Hansen, V. L. (1992). Regional non-coaxial deformation on Venus: Evidence from western Itzpapalotl tessera. Abstracts of the Lunar and Planetary Science Conference, volume *23*, page 479. Houston, Texas.

Hansen, V. L. (2000). Geologic mapping of tectonic planets. *Earth and Planetary Science Letters*, *176*(3-4), 527–542. https://doi.org/10.1016/S0012-821X(00)00017-0

Hansen, V. L. (2005). Venus's shield-terrain. *Geological Society of America Bulletin*, *117*, 808–822. https://doi.org/10.1130/B256060.1

Hansen, V. L. (2006). Geologic constraints on crustal plateau surface histories, Venus: The lava pond and bolide impact hypotheses. *Journal of Geophysical Research*, *111*, E11010. https://doi.org/10.1029/2006JE002714

Hansen, V. L. (2009). Geologic map of the Niobe Planitia quadrangle (V-23), Venus: U.S. *Geological Survey Scientific Investigations Map* 3025, 1:5M, https://pubs.er.usgs.gov/publication/sim3025

Hansen, V. L. (2018). Global tectonic evolution of Venus. *Phylosophysical Transactions of the Royal Society A*, *376*, 20170412. https://doi.org/10.1098/rsta.2017.0412

Hansen, V. L., & López, I. (2010). Venus records a rich early history. *Geology*, *38*(4), 311–314. https://doi.org/10.1130/G30587.1

Hansen, V. L., & López, I. (2018). Mapping of geologic structures in the Niobe-Aphrodite map area of Venus: Unraveling the history of tectonic regime change. *Journal of Geophysical Research: Planets*, *123*, 1760–1790. https://doi.org/10.1029/2018JE005566

Hansen, V. L., & López, I. (2020). Geologic map of Aphrodite map area (AMA; I-2476), Venus. *Earth and Space Science Open archive*. Preprint on https://doi.org/10.1002/essoar.10502475.1

Hansen, V. L., & Olive, A. (2010). Artemis, Venus: The largest tectonomagmatic feature in the solar system? *Geology*, *38*(5), 467–470. https://doi.org/10.1130/G30643.1

Hansen, V. L., Phillips, R. J., Willis, J. J., & Ghent, R. R. (2000). Structures in tessera terrain, Venus: Issues and answers. *Journal of Geophysical Research*, *105*(E2), 4135–4152. https://doi.org/10.1029/1999JE001137

Hansen, V. L., & Tharalson, E. R. (2014). Geologic map of the Agnesi quadrangle (V-45), Venus: *U.S. Geological Survey Scientific Investigations Map* 3250, 1:5M, https://pubs.er.usgs.gov/publication/sim3250

Hansen, V. L., & Willis, J. J. (1996). Structural analysis of a sampling of tesserae: Implications for Venus geodynamics. *Icarus*, *123*(2), 296–312. https://doi.org/10.1006/icar.1996.0159

Hansen, V. L., & Willis, J. J. (1998). Ribbon terrain formation, southwestern Fortuna Tessera, Venus—Implications for lithosphere evolution. *Icarus*, *132*(2), 321–343. https://doi.org/10.1006/icar.1998.5897

Hansen, V. L., & Young, D. A. (2007). Venus's evolution: A synthesis. In M. Cloos, W. D. Carlson, M. C. Gilbert, J. G. Liou, & S. S. Sorensen (Eds.), *Convergent margin terranes and 6 associated regions—A Tribute to W.G* (pp. 255–273). Ernst: Geological Society of America. https://doi.org/10.1130/2006.2419(13

Hauck, S. A., Phillips, R. J., & Price, M. H. (1998). Venus: Crater distribution and plains resurfacing models. *Journal of Geophysical Research*, *103*(E6), 13,635–13,642. https://doi.org/10.1029/98JE00400

Herrick, R. R., & MacGovern, P. J. (2000). Kunhild and Ereshkigal, an extinct hot-spot región on Venus. *Geophysical Research Letters*, *27*, 839–842. https://doi.org/10.1029/1999GL008395

Herrick, R. R., & Rumpf, M. E. (2011). Post-impact modification by volcanic or tectonic processes as the rule, not the exception, for Venusian craters. *Journal of Geophysical Research*, *116*, E02004. https://doi.org/10.1029/2010JE003722

Herrick, R. R., & Sharpton, V. L. (2000). Implications from stereo-derived topography of Venusian impact craters. *Journal of Geophysical Research*, *105*(E8), 20,245–20,262. https://doi.org/10.1029/1999JE001225

Herrick, R. R., Sharpton, V. L., Malin, M. C., Lyons, S. N., & Feely, K. (1997). Morphology and morphometry of impact craters. In D. M. Hunten, & R. J. Phillips (Eds.), *Bouger, S.W* (pp. 1015–1046). Venus II: Tucson: University of Arizona Press.

Ivanov, M. A., & Head, J. W. (1996). Tessera terrain on Venus: A survey of the global distribution, characteristics, and relation to surrounding units from Magellan data. *Journal of Geophysical Research*, *101*(E6), 14,861–14,908. https://doi.org/10.1029/96JE01245

Ivanov, M. A., & Head, J. W. (2004). Geologic map of the Atalanta Planitia Quadrangle (V-4), Venus. *U.S. Geological Survey Scientific Investigations* I-2792. http://pubs.usgs.gov/imap/i2792

Ivanov, M. A., & Head, J. W. (2005). Geologic map of the Nemesis Tessera Quadrangle (V-13), Venus. *U.S. Geological Survey Scientific Investigations* I-2870. http://pubs.usgs.gov/imap/i2870

Ivanov, M. A., & Head, J. W. (2008). Geologic map of the Meskhent Tessera Quadrangle (V-3), Venus. *U.S. Geological Survey Scientific Investigations* I-3018. http://pubs.usgs.gov/imap/i3018

Ivanov, M. A., & Head, J. W. (2011). Global geological map of Venus. *Planetary and Space Science*, *59*(13), 1559–1600. https://doi.org/10.1016/j.pss.2011.07.008

Ivanov, M. A., & Head, J. W. (2015a). Volcanically embayed craters on Venus: Testing the catastrophic and equilibrium resurfacing models. *Planetary and Space Science*, *106*, 116–121. https://doi.org/10.1016/j.pss.2014.12.004

Ivanov, M. A., & Head, J. W. (2015b). The history of tectonism on Venus: A stratigraphic analysis. *Planetary and Space Science*, *113-114*, 10–32. https://doi.org/10.1016/j.pss.2015.03.016

Izenberg, N. R., Arvidson, R. E., & Phillips, R. J. (1994). Impact crater degradation on Venusian plains. *Geophysical Research Letters*, *21*(4), 289–292. https://doi.org/10.1029/94GL00080

Jones, A. P., & Pickering, K. T. (2003). Evidence for aqueous fluid-sediment transport and erosional processes on Venus. *Journal of the Geological Society of London*, *160*(2), 319–327. https://doi.org/10.1144/0016-764902-111

Kirk, R. L., & Chadwick, D. J. (1994). Splotches on Venus: Distribution, properties and classification. *Abstracts of the 25th Lunar and Planetary Science Conference*. p.705. Houston, TX.

Kirk, R. L., Soderblom, L., & Lee, E. (1992). Enhanced visualization for interpretation of Magellan radar data—Supplement to the Magellan special issue. *Journal of Geophysical Research*, *97*, 16,371–16,380. https://doi.org/10.1029/92JE01785

Komatsu, G., & Baker, V. R. (1994). Meander properties of venusian channels. *Geology*, *22*(1), 67–70. https://doi.org/10.1130/0091-7613(1994)022<0067:MPOVC>2.3.CO;2

Kreslavsky, M. A., Ivanov, M. A., & Head, J. W. (2015). The resurfacing history of Venus: Constraints from buffered crater densities. *Icarus*, *250*, 438–450. https://doi.org/10.1016/j.icarus.2014.12.024

Lang, N. P., & Hansen, V. L. (2006). Venusian channel formation as a subsurface process. *Journal of Geophysical Research*, *111*, E04001. https://doi.org/10.1029/2005JE002629

Lang, N. P., & Hansen, V. L. (2008). Geologic map of the Greenaway quadrangle (V–24), Venus: U.S. Geological Survey Scientific Investigations Map 3089, scale 1:5,000,000 (http://pubs.usgs.gov/sim/3089).

López, I. (2011). Embayed intermediate volcanoes on Venus: Implications for the evolution of the volcanic plains. *Icarus*, *213*(1), 73–85. https://doi.org/10.1016/j.icarus.2011.02.022

López, I., & Hansen, V. L. (2020). Niobe Planitia Region (I–2467), Venus: base maps for geologic mapping. [Data set]. Zenodo. http://doi.org/10.5281/zenodo.3712688

Maltman, A. (1990). *Geological maps: An introduction* (p. 184). Buckingham U.K: Open University Press. https://doi.org/10.1007/978-1-4684-6662-1

McGill, G. E., & Campbell, B. A. (2004). Ages of Venusian ridge belts relative to regional plains. *Lunar and Planetary Science Conference XXXVI*. Abstract #1143. Houston, TX.

McKinnon, W. B., Zahnle, K. J., Ivanov, B. A., & Melosh, H. J. (1997). Cratering on Venus: Models and observations. In S. W. Bouger, D. M. Hunten, & R. J. Phillips (Eds.), (pp. 969–1014). Venus II: Tucson: University of Arizona Press.

O'Rourke, J. G., & Korenaga, J. (2015). Thermal evolution of Venus with argon degassing. *Icarus*, *260*, 128–140. https://doi.org/10.1016/j.icarus.2015.07.009

Okubo, C. H., & Martel, S. J. (1998). Pit crater formation on Kilauea volcano, Hawaii. *Journal of Volcanology and Geothermal Research*, *86*(1-4), 1–8. https://doi.org/10.1016/S0377-0273(98)00070-5

Pavri, B., Head, J. W., Klose, K. B., & Wilson, L. (1992). Steep-sided domes on Venus: Characteristics, geologic setting, and eruption conditions from Magellan data. *Journal of Geophysical Research*, *97*(E8), 13,445–13,478. https://doi.org/10.1029/92JE01162

Phillips, R. J., & Hansen, V. L. (1994). Tectonic and magmatic evolution of Venus. *Annual Review of Earth and Planetary Sciences*, *22*(1), 597–656. https://doi.org/10.1146/annurev.ea.22.050194.003121

Phillips, R. J., & Hansen, V. L. (1998). Geological evolution of Venus: Rises, plains, plumes and plateaus. *Science*, *279*(5356), 1492–1497. https://doi.org/10.1126/science.279.5356.1492

Phillips, R. J., & Izenberg, N. R. (1995). Ejecta correlations with spatial crater density and Venus resurfacing history. *Geophysical Research Letters*, *22*(12), 1517–1520. https://doi.org/10.1029/95GL01412

Phillips, R. J., Raubertas, R. F., Arvidson, R. E., Sarkar, I. C., Herrick, R. R., Izenberg, N., & Grimm, R. E. (1992). Impact crater distribution and the resurfacing history of Venus. *Journal of Geophysical Research*, *97*(E10), 15,923–15,948. https://doi.org/10.1029/92JE01696

Price, M., & Suppe, J. (1995). Constraints on the resurfacing history of Venus from the hypsometry and distribution of volcanism, tectonism, and impact craters. *Earth, Moon, and Planets*, *71*(1–2), 99–145. https://doi.org/10.1007/BF00612873

Reese, C. C., Solomatov, V. S., & Orth, C. P. (2007). Mechanisms for cessation of magmatic resurfacing on Venus. *Journal of Geophysical Research*, *112*, E04S04. https://doi.org/10.1029/2006JE002782

Romeo, I. (2013). Monte Carlo models of the interaction between impact cratering and volcanic resurfacing on Venus: The effect of the Beta-Atla-Themis anomaly. *Planetary and Space Science*, *87*, 157–172. https://doi.org/10.1016/j.pss.2013.07.010

Romeo, I., & Turcotte, D. L. (2010). Resurfacing on Venus. *Planetary and Space Science*, *58*(10), 1374–1380. https://doi.org/10.1016/j.pss.2010.05.022

Ruiz, J. (2007). The heat flow during formation of ribbon terrains on Venus. *Planetary and Space Science*, *55*, 2063–2070. https://doi.org/10.1016/j.icarus.204.11.007

Sandwell, D. T., Johnson, C. L., Bilotti, F., & Suppe, J. (1997). Driving forces for limited tectonics on Venus. *Icarus*, *129*(1), 232–244. https://doi.org/10.1006/icar.1997.5721

Schaber, G. G., Strom, R. G., Moore, H. J., Soderblom, L. A., Kirk, R. L., Chadwick, D. J., et al. (1992). Geology and distribution of impact craters on Venus: What are they telling us? *Journal of Geophysical Research*, *97*(E8), 13,257–13,302. https://doi.org/10.1029/92JE01246

Schaller, C. J., & Melosh, H. J. (1998). Venusian ejecta parabolas: Comparing theory with observations. *Icarus*, *131*(1), 123–137. https://doi.org/10.1006/icar.1997.5855

Schultz, R. A., Okubo, C. H., Goudy, C. L., & Wilkins, S. J. (2004). Igneous dikes on Mars revealed by Mars orbiter laser altimeter topography. *Geology*, *32*(10), 889–892. https://doi.org/10.1130/G20548.1

Senske, D. A., Schaber, G. G., & Stofan, E. R. (1992). Regional topographic rises on Venus: Geology of Western Eistla Regio and comparison to Beta Regio and Atla Regio. *Journal of Geophysical Research*, *97*(E8), 13,395–13,420. https://doi.org/10.1029/92JE01167

Shalygin, E. V., Markiewicz, W. J., Basilevsky, A. T., Titov, D. V., Ignatiev, N. I., & Head, J. W. (2015). Active volcanism on Venus in the Ganiki Chasma rift zone. *Geophysical Research Letters*, *42*, 4762–4769. https://doi.org/10.1002/2015GL064088

Shankar, B. (2008). A global survey of circular lows: A subset of Coronae, Venus. M.S. Thesis, 87 pp. University of Minnesota Duluth, MN.

Skinner, J. A., & Tanaka, K. L. (2003). How should map units be defined? *Lunar and Planetary Science Conference XXXIV*. Abstract #2100. Houston, TX.

Smrekar, S. E., & Stofan, E. R. (1999). Origin of corona-dominated topographic rises on Venus. *Icarus*, *139*(1), 100–115. https://doi.org/10.1006/icar.1999.6090

Solomatov, V. S., & Moresi, L. N. (1996). Stagnant lid convection on Venus. *Journal of Geophysical Research*, *101*(E2), 4737–4753. https://doi.org/10.1029/95JE03361

Stofan, E. R., Anderson, S. W., Crown, D. A., & Plaut, J. J. (2000). Emplacement and composition of steep-sided domes on Venus. *Journal of Geophysical Research*, *105*(E11), 26,757–26,771. https://doi.org/10.1029/1999JE001206

Stofan, E. R., Brian, A. W., & Guest, J. E. (2005). Resurfacing styles and rates on Venus: Assessment of 18 Venusian quadrangles. *Icarus*, *173*, 312–321. https://doi.org/10.1016/j.icarus.2004.08.004

Stofan, E. R., Senske, D. A., & Michaels, G. (1993). Tectonic features in Magellan data. In P. J. Ford, J. Plaut, C. M. Wietz, & 5 others (Eds.), *Guide to Magellan image interpretation* (pp. 93–108). Pasadena, Calif: National Aeronautics and Space Administration Jet Propulsion Laboratory.

Strom, R. G., Schaber, G. G., & Dawson, D. D. (1994). The global resurfacing of Venus. *Journal of Geophysical Research*, *99*(E5), 10,899–10,926. https://doi.org/10.1029/94JE00388

Tanaka, K. L., Schaber, G. G., Chapman, M. G., Stofan, E. R., Campbell, D. B. Davis, P. A., et al. (1993). The Venus geologic mappers' handbook (2nd ed.). 68 p. U.S. Geological Survey Open-File Report 94–438.

Tanaka, K. L., Skinner, J. A., & Hare, T. M. (2010). Planetary geologic mapping handbook. Abstracts of the Annual Meeting of Planetary Geologic Mappers, Flagstaff, AZ, 2010; p. 1-20; NASA/CP-2010-217041.

Turcotte, D. L. (1993). An episodic hypothesis for Venusian tectonics. *Journal of Geophysical Research*, *98*(E9), 17,061–17,068. https://doi.org/10.1029/93JE01775

Turcotte, D. L., Morein, G., & Malamud, B. D. (1999). Catastrophic resurfacing and episodic subduction on Venus. *Icarus*, *139*(1), 49–54. https://doi.org/10.1006/icar.1999.6084

Waltham, D., Pickering, K. T., & Bray, V. J. (2008). Particulate gravity currents on Venus. *Journal of Geophysical Research*, *113*, E02012. https://doi.org/10.1029/2007JE002913

Watters, T. R. (1988). Wrinkle ridge assemblages on the terrestrial planets. *Journal of Geophysical Research*, *93*, 236–254. https://doi.org/10.1029/JB093ib09p10236

Weitz, C. M. (1993). Impact craters. In P. J. Ford, J. Plaut, C. M. Wietz, & 5 others (Eds.), *Guide to Magellan image interpretation* (pp. 75–92). Pasadena, Calif: National Aeronautics and Space Administration Jet Propulsion Laboratory.

Whitten, J. L., & Campbell, B. A. (2016). Recent volcanic resurfacing of Venusian craters. *Geology*, *44*(7), 519–522. https://doi.org/10.1130/G37681.1

Wilhelms, D. E. (1972). Geologic mapping of the second planet. *U.S. Geological Survey Interagency Report,* Astrogeology, 55 pp.

Wilhelms, D. E. (1990). Geologic mapping. In R. Greeley, & R. M. Batson (Eds.), *Planetary mapping* (pp. 208–260). New York: Cambridge University Press.

Williams-Jones, G., Williams-Jones, A. E., & Stix, J. (1998). The nature and origin of Venusian Canali. *Journal of Geophysical Research*, *103*(E4), 8545–8555. https://doi.org/10.1029/98JE00243

Young, D. A., & Hansen, V. L. (2003). Geologic map of the Rusalka Planitia Quadrangle (V-25), Venus. *U.S. Geological Survey Scientific Investigations Map* I-2783, http://pubs.usgs.gov/imap/i2783/

Young, D. A., & Hansen, V. L. (2005). Poludnista Dorsa, Venus: History and context of a deformation belt. *Journal of Geophysical Research*, *110*, E03001. https://doi.org/10.1029/2004JE002280

Zimbelman, J. R. (2001). Image resolution and evaluation of genetic hypotheses for planetary landscapes. *Geomorphology*, *37*(3-4), 179–199. https://doi.org/10.1016/S0169-555X(00)00082-9